

# AES 670 Satellite Remote Sensing Final Project

Mitchell Dodson

April 23, 2023

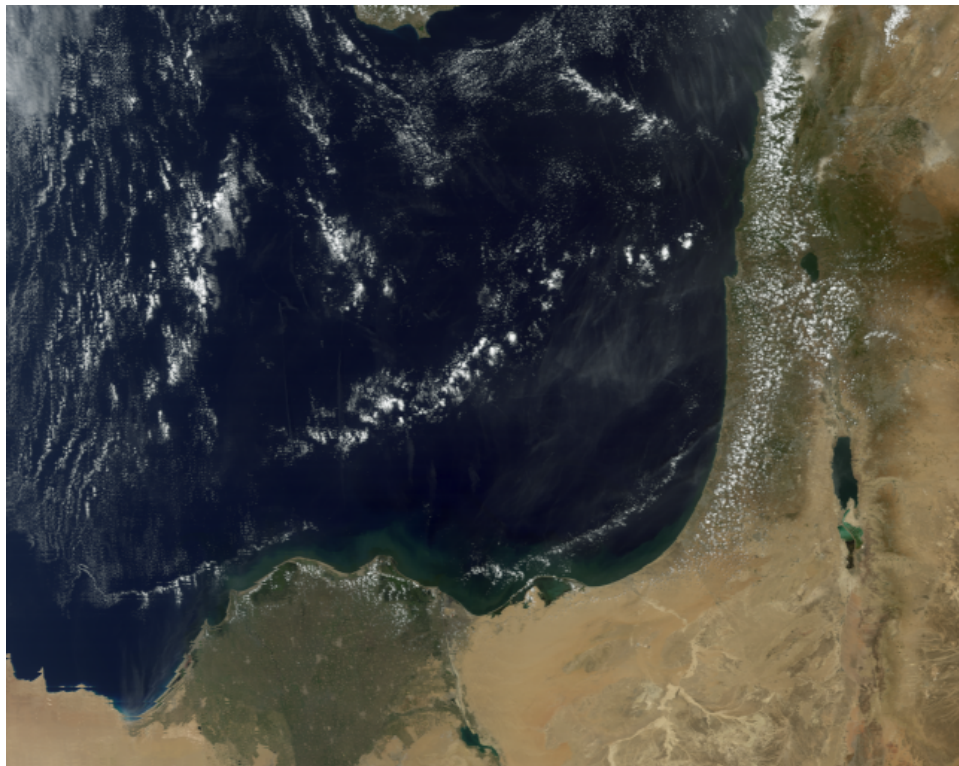


Figure 1: MODIS Truecolor image of my chosen region.

## 1 Abstract

In this project I use MODIS L1b (MOD012KM) data to perform surface classification and analysis of a region including the Southeast Mediterranean, the Nile River delta, and The Levant. To characterize this region, I develop several RGBs, a custom thresholding technique, and assign surface types with unsupervised K-means classification and supervised maximum-likelihood classification (MLC) algorithms. The surface types I focus on are (1) ice clouds, (2) water clouds, (3) vegetation, (4) surface water, and (5) arid ground, though several other surface types were identified during analysis. Correlation statistics and spectral response curves of surface classes are provided for each classification result. I will also use this report as documentation for the Python package I'm developing, as outlined in section 2.

## 2 Code comment

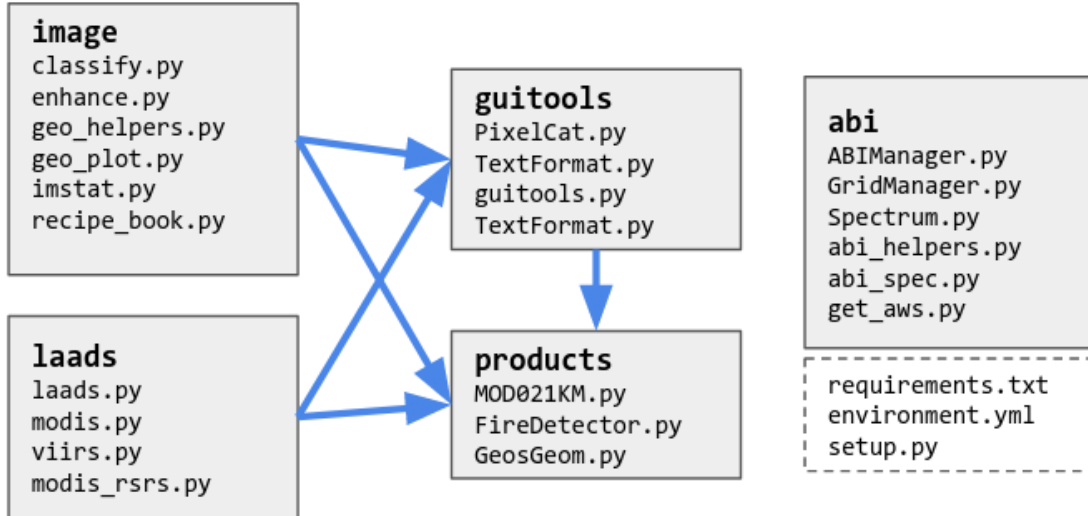


Figure 2: Module layout and dependency graph for my Python package for satellite data acquisition and analysis. The package is organized into modules containing generalized methods for a variety of tasks, as well as several classes for higher-level analysis. In accordance with Python naming convention, class files are capitalized and modules containing only methods are lowercase. My repository can be installed and imported like any other Python package, and is available on GitHub at <https://github.com/Mitchell-D/aes670hw2/>

One of my major goals for graduate school is to collect code I write for classes and research into a reusable package of software tools with a common architecture and a minimal number of dependencies, which I ultimately want to develop into an ongoing open-source software project. This class has enabled me to make significant headway on my goal, so this report will serve as both a surface analysis of my region and a demonstration of my software. Figure 2 shows the layout of my package, which is currently called `aes670hw2` (subject to renaming soon). The package and its dependencies can be installed manually with `pip install /path/to/aes670hw2`, or with `conda-forge` using the included `environment.yml` file. Any of the sub-modules can be imported directly from the package, for example `from aes670hw2 import enhance as enh`.

Software development is a balancing act between usability and re-usability. “Low-level” operations like N-dimensional histogram matching must be complicated enough to be useful to specialized tasks without the need for extra infrastructure code, and “high-level” methods like getting user input at runtime with a live-rendered RGB must be general enough to be used for a variety of data circumstances. As such, I’m keeping a wide range potential future use cases in mind for each every module, and attempting to separate the methods within each module into a reusable collection of sub-tasks. For instance, `enhance.histogram_match` is a relatively high-level method that takes two equally-shaped 2d or 3d arrays and histogram-matches the first two axes of the first array to the first two axes of the second array in a provided number of bins. This method is only 19 lines long since it subsequently depends on `enhance.get_cumulative_hist`, `enhance.get_pixel_counts`, `enhance.norm_to_uint`, and other sub-tasks that are reusable for a variety of other purposes.

I have a long list of future plans for this project, which include developing API wrappers for data sources other than the LAADS DAAC and NOAA AWS buckets, adapting the `products.MOD021KM` class design to support any gridded dataset, and an asynchronous process queue to enable multiple simultaneous OpenCV2 windows. My codebase currently exceeds 7,500 lines of Python, which includes detailed internal documentation for every method. The following tables provide an overview of each module's purpose.

| Module                | Purpose   |
|-----------------------|---|
| <code>products</code> | The <code>products</code> module contains three classes: <code>FireDetector.py</code> , <code>GeosGeom.py</code> , and <code>MOD021KM.py</code> . The first is a relatively simple class that executes the fire detection algorithm outlined in (Flasse & Ceccato, 1996) [1] with optional custom thresholds, and which only depends on numpy. The second is also a fairly simple but highly generalized class that generates surface latitude/longitude and pixel/sun/sensor trigonometry arrays from basic sun/satellite geometry information for any geostationary satellite. The third, <code>MOD021KM.py</code> , is however a very abstract class that provides a wide variety of methods for interfacing with and analyzing MODIS L1b data in the MOD021KM or MYD021KM formats. The class includes static methods for finding, downloading, parsing, calculating, and subsetting a user-provided set of L1b MODIS reflectance and brightness temperature bands to a geographic range. Since MOD021KM objects can be easily created from a L1b HDF, instances of the MOD021KM class are built on and enforce the principles that the underlying band data they are initialized with cannot change, that all contained datasets have an identical shape, and that any band composite recipe can be expressed as a directed tree graph of other composite recipes it depends on, all of which must ultimately terminate with raw band data as a “leaf node” argument. This enables the object to repeatably dynamically evaluate a hierarchy of recipe dependencies at runtime. For example, the user may provide the MOD021KM object a <code>guitools.Recipe</code> object with an arbitrary function (ie histogram equalization/matching, an analytic function, a 5-band composite), a string label, and a list of band or recipe labels corresponding to the function’s arguments. By referencing the label, the new Recipe can be enhanced, histogram-analyzed, rendered as an RGB, or used for threshold selection, classification, fourier analysis, etc. All of these operations can be accessed by calling a single respective method of the MOD021KM instance. The MOD021KM object also contains wrappers on many other methods for GUI selection and enhancement, K-means and migrating means classification, data mask creation/manipulation/comparison, etc, which will be used often throughout this report. |
| <code>abi</code>      | The <code>abi</code> module is mostly adapted from one of my old codebases, and isn’t integrated with the rest of the package. It contains methods for querying the NOAA AWS Bucket for GOES East and GOES West ABI and GLM data ( <code>get_aws.py</code> ), subsetting, projecting, and aligning geolocated arrays ( <code>abi_helpers.py</code> and <code>GridManager.py</code> ), and for rendering animations and performing a variety of analyses on time series of ABI data ( <code>ABIManager.py</code> ).  |

| Module   | Purpose   |
|----------|---|
| image    | The <code>image</code> module contains sub-modules with methods for performing enhancement and other pixelwise operations on general 2d and 3d arrays ( <code>enhance.py</code> ), plotting continuous and discrete 1d, 2d, and 3d data in a variety of formats with a common configuration style ( <code>geo_plot.py</code> ), manipulating and interpolating 2d and 3d arrays in multiple coordinate systems ( <code>geo_helpers.py</code> ), performing histogram analysis, equalization, and matching on arbitrary 2d and 3d arrays ( <code>enhance.py</code> ), applying arbitrary convolutional kernels to arrays with several hardcoded options, running my fast-fourier implementation and applying user-defined frequency masks ( <code>enhance.py</code> ), and contains a variety of hardcoded RGB recipes ( <code>recipe_book.py</code> ). This module has no dependencies that aren't installed by default in Python <code>wheel</code> .  |
| laads    | The <code>laads</code> module currently consists of 3 main sub-modules: <code>laads.py</code> , <code>viirs.py</code> , and <code>modis.py</code> . The <code>laads.py</code> sub-module contains a collection of abstract methods for querying the Earth Observing System's LAADS DAAC archive's REST API, enabling the user to retrieve information about, search for, and download any available product with optional geographic and time constraints. The <code>viirs.py</code> and <code>modis.py</code> sub-modules use <code>laads.py</code> to search for user-specified L1b or L2 swaths at any resolution, and provide methods for parsing their respective data files into a common format consisting minimally of a tuple of requested band arrays, and a list of dictionaries corresponding to each band with meta-information such as conversion coefficients, units, and center wavelengths. These methods also optionally provide coordinate reference, sun/satellite geometry, and terrain information if available.  |
| guitools | The <code>guitools</code> module contains the self-titled sub-module <code>guitools.py</code> as well as two specialized classes <code>PixelCat.py</code> and <code>TextFormat.py</code> . The main dependency of this module is the Python wrapper for OpenCV2, which <code>guitools.py</code> uses to provide functions to get user input with GUI interfaces and to perform a variety of RGB rendering operations. The sub-module contains GUI methods with interactive windows prompting the user to select a group of pixels in an image, select a rectangular or circular region of an image, or select a scalar value for the image. The latter method re-renders the image in the window using an arbitrary user-defined function of the array and a scalar variable. This function can be defined to let the user interactively choose contrast, gamma, histogram mean, and value thresholds for an arbitrary scalar array. <code>guitools.py</code> also contains lower-level methods for rendering a scalar array as an RGB using linear functions of hue, saturation, and value, returning a PNG as a numpy array, generating an array of unique colors, and getting an RGB array with normally-distributed color histograms according to user-defined means and standard deviations for each channel. The <code>PixelCat</code> class is a high-level class offering wrappers on GUI utilities for performing fourier analysis on, enhancing, and selecting pixels from arbitrary RGB arrays, and the <code>TextFormat</code> class colors and formats strings using ANSI escape codes for pretty terminal printing. |

### 3 Data and domain of analysis

---

**NOTE:** In order to prevent confusion between class and object methods, I will refer to static class methods with the notation `MOD021KM.static_method`, and methods that must be called on an instance of the object with the notation `subgrid.object_method`, where `subgrid` is presumed to be a `MOD021KM` object with all the needed bands loaded. Instances may be initialized with an HDF by calling the static method `subgrid = MOD021KM.from_hdf(l1b_hdf, l1b_bands)`. Existing MOD021KM objects can be stored as a pickle binary file with `subgrid.make_pkl(pkl_path)`, and subsequently retrieved from the file with `subgrid = MOD021KM.from_pkl(pkl_path)`.

## 3 Data and domain of analysis

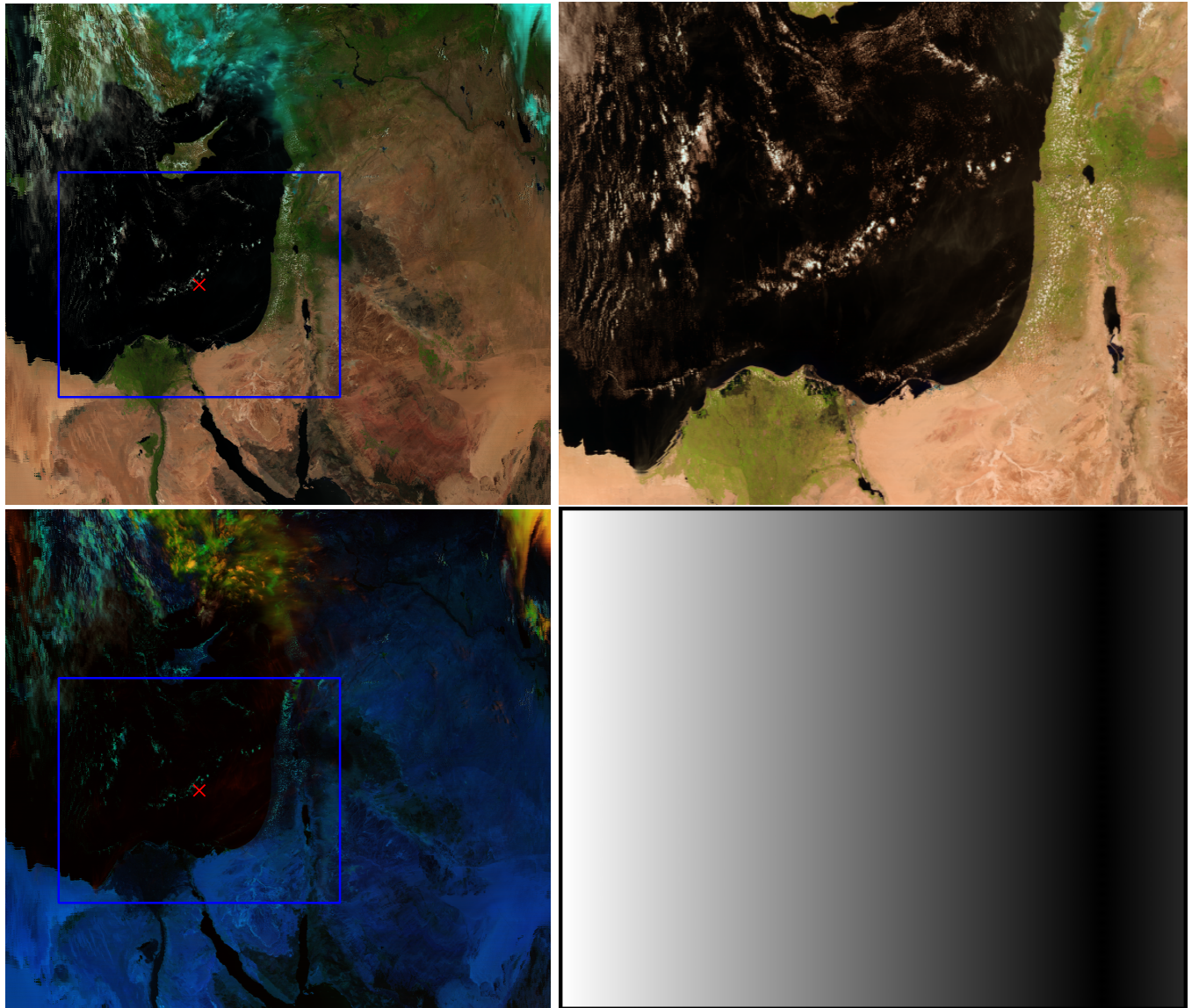


Figure 3: Top: Natural-color RGBs of a wide view of the location of my region and a focused view of the subgrid I used for analysis, which features the East Mediterranean, the Southern tip of Cyprus, and the Nile River delta on the left, with the Sinai Peninsula and the Levant on the Right. Bottom: Daytime cloud phase RGB composite of a broad view of my region, and a scalar mapping of the viewing zenith angle within my subgrid, which ranges from 0° (NADIR; black) to 52° (white) from vertical.

### 3 Data and domain of analysis

---

Figure 3 provides context on the region that I selected, which is centered on 32.41° East, 32.99° North and covers a total surface area of 528,689.3km. The MODIS L1b granule that includes my image was captured by the Terra platform on May 10, 2019 at 0829z, or 10:29am local time in Egypt. I downloaded the L1b data with `MOD021KM.download_granule`, providing the desired platform, target time, and geographic range of my domain, then initialized a MOD021KM object with the HDF file and a list of all the bands in Table 2 using `subgrid = MOD021KM.from_hdf`.

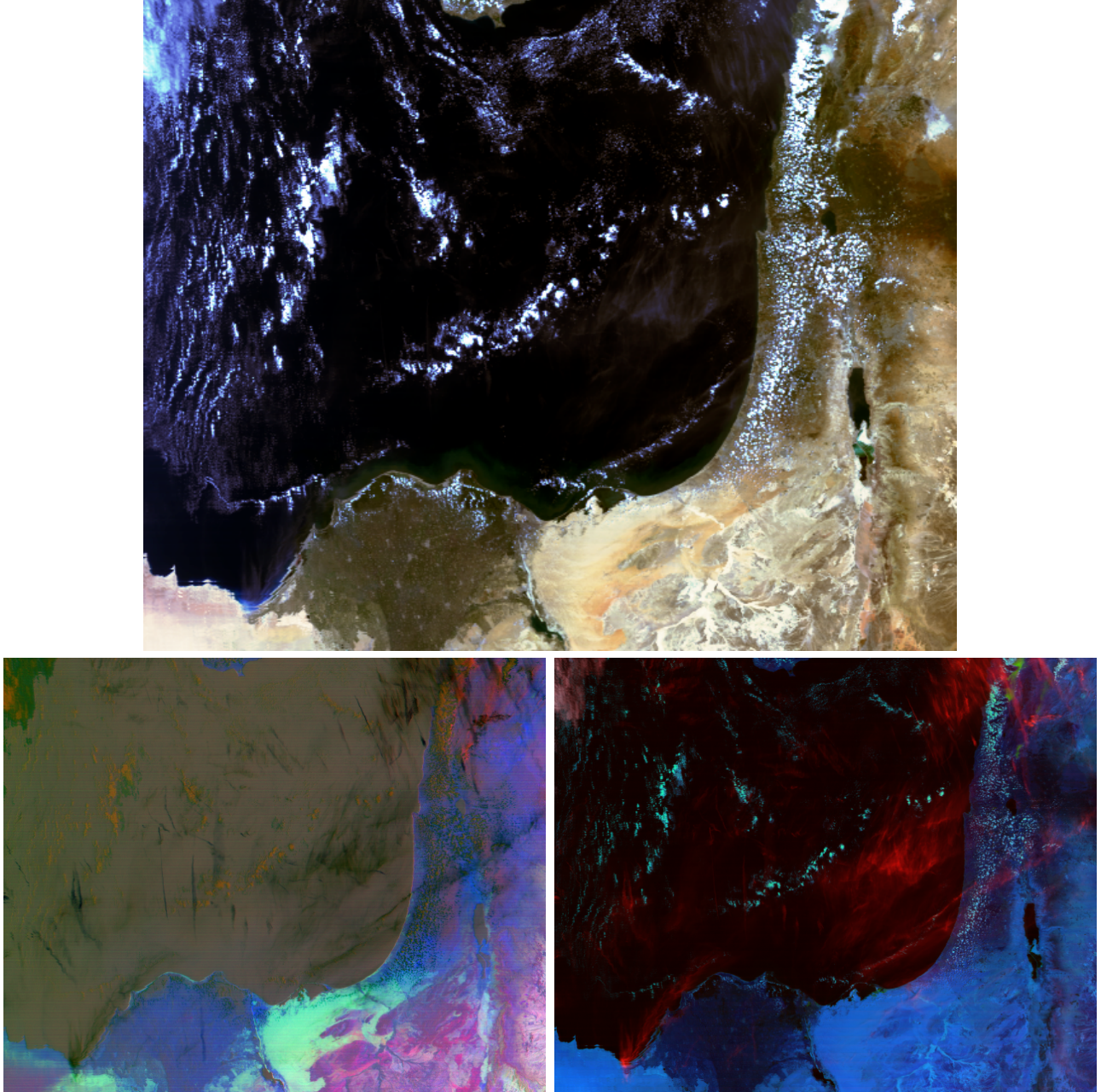


Figure 4: Top: histogram-equalized and gamma-enhanced true color RGB. Bottom: gamma-enhanced dust RGB [2] and daytime cloud-phase RGB [3]. Each of these recipes are loaded by default in `MOD021KM` objects with the labels “CUSTOMeq,” “DUST,” and “DCP.” They were generated with enhancement values manually chosen using the GUI launched by `subgrid.get_rgb("DUST", choose_gamma=True)` for each RGB label.

### 3 Data and domain of analysis

---

| Dust RGB channels             | Description   |
|-------------------------------|---|
| RED=norm( $12 - 11\mu m$ )    | Cloud and dust optical thickness. Optically thick clouds and clear-sky land surfaces have values near zero, which are normalized to become bright since channel difference values generally range from $-5^{\circ}C$ to $1^{\circ}C$ . Low values indicate more attenuation by water vapor than $12\mu m$ . |
| GREEN=norm( $11 - 8.6\mu m$ ) | Cloud particle phase and land surface emissivity. The 8.6. Water-phase clouds and surfaces with low emissivity have high values. Atmospheric columns with more water vapor absorption will also be tinted green.  |
| BLUE=norm( $11\mu m$ )        | LWIR window for cloud-top and land temperature.   |
| Day-cloud RGB channels        | Description   |
| RED=norm( $1.38\mu m$ )       | Cirrus cloud detection due to strong water vapor attenuation at mid and low layers  |
| GREEN=norm( $.64\mu m$ )      | Visible band for cloud optical thickness  |
| BLUE=norm( $1.64\mu m$ )      | Cloud-phase distinction; Water droplets are reflective, but ice particles strongly absorb.  |

Table 1: Recipes for false-color RGBs in Figure 4. Note that the sources for these RGB recipes limit data to certain ranges and apply specific gamma enhancements. Those values aren't included here since they can be selected to suit a task at runtime with `subgrid.data("label", choose_contrast=True, choose_gamma=True)`.

The histogram-equalized true color RGB in Figure 4 clearly shows the transition between the barren sandy desert surrounding the Nile Delta and the exposed rock and scrub of the Sinai peninsula, which is corroborated by corresponding light blue/green and magenta surfaces in the dust RGB. The GREEN band of the dust RGB recipe is the  $11 - 8.6\mu m$  LWIR channel difference, which is highly sensitive to the emissivity properties of barren land surfaces [4]. Bare stone and soil generally have an emissivity  $\epsilon \approx .92$ , and sand has an emissivity  $\epsilon \approx .89$ , which causes the brightness temperature of sand to appear artificially cool in the  $8.6\mu m$  band. This inflates the channel difference over sandy surfaces, hence the green hue of that region in the dust RGB.

The  $11 - 8.6\mu m$  channel difference in the dust GREEN channel also contributes more heavily to water-phase clouds than ice-phase clouds due to the much higher emissivity of ice than water, which explains the green tint of low-level water clouds in the RGB. The dust RGB's RED band is the  $12 - 11\mu m$  channel difference, which takes advantage of the additional water vapor attenuation in the  $12\mu m$  band to quantify cloud optical depth, as the ratio of surface emissions absorbed at  $12\mu m$  to emissions absorbed at  $11\mu m$  slightly increases with the amount of water vapor in the atmospheric column. Thus, the tan/orange clouds in the RGB correspond to optically-thick water and mixed-phase clouds, and the dark green pixels correspond to optically-thin and sub-pixel water clouds. The BLUE channel of the dust RGB is simply the  $11\mu m$  LWIR window channel, so cirrus clouds are black due to their high emissivity, low optical depth and cold temperature.

The daytime cloud-phase RGB assigns the  $1.38\mu m$  cirrus band to RED, the  $6.4\mu m$  red band to GREEN, and the  $1.64\mu m$  cloud-phase band to BLUE. Since water absorbs

### 3 Data and domain of analysis

---

very strongly in the NIR range, there is stark contrast between the Mediterranean sea surface, low-level and sub-pixel water clouds, and high-level cirrus clouds. The red streaks throughout the center of the image suggest pervasive thin cirrus contamination over the sea and Israel. Compared to the large-scale daytime cloud phase RGB in Figure 3, it’s clear that these cirrus are very optically thin, which poses challenges in later analysis.

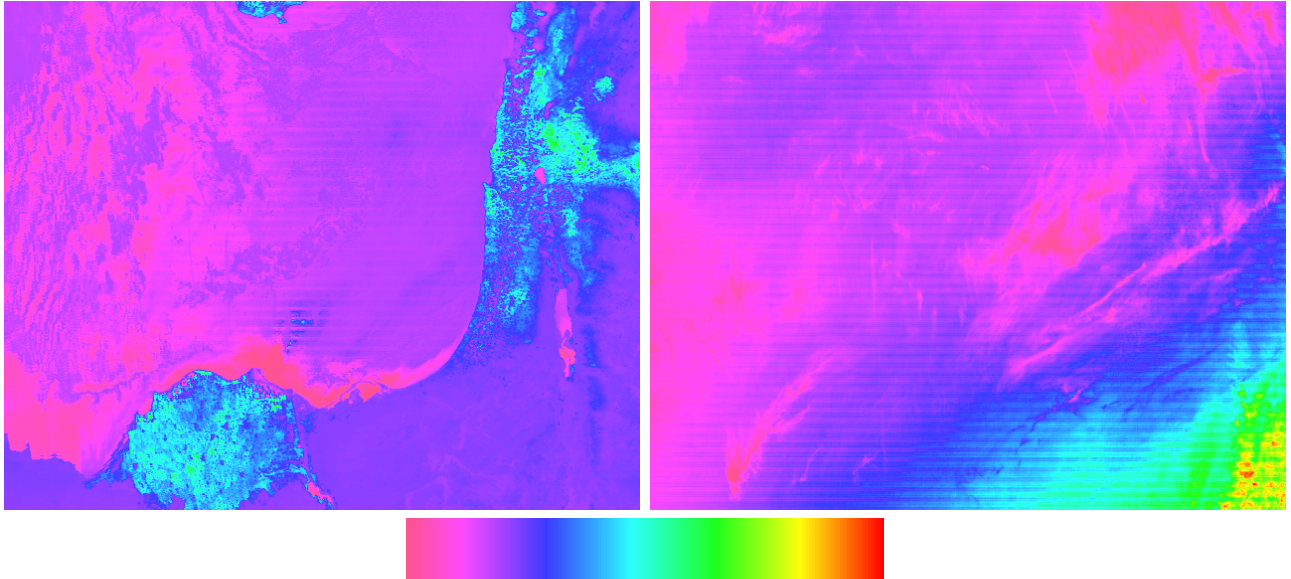


Figure 5: Left: gamma-enhanced heatmap of NDVI (using  $.86\mu m$  NIR and  $.64\mu m$  RED bands). Right: gamma-enhanced heatmap of MODIS band 28 ( $7.3\mu m$ ) brightness temperatures. Both images are normalized to the scale of the color bar below low values in magenta and high values in red. These were generated by `geo_plot.generate_raw_image` using RGBs from `guitools.scal_to_rgb`, for example: `guitools.scal_to_rgb(subgrid.data("ndvi",choose_gamma=True))`. Hue, saturation, and value ranges for the RGB-mapped scalar array can be optionally provided.

The left image in Figure 5 shows a heatmap of vegetation on the banks of the Mediterranean, which captures the arid climate of the Sinai peninsula, the sparse vegetation of the Jordanian highlands, and the highly-vegetated Nile Delta and Levant regions, as well as the southern tip of Cyprus. The right image shows the  $7.175 - 7.475\mu m$  mid-level water vapor band, which features cold brightness temperatures indicating a steep gradient of vapor content increasing to the Northwest over the sea. Water vapor is especially concentrated along the West edge of the region, which is further occluded by sub-pixel clouds and panoramic distortion as the true color RGB in Figure 4 and viewing zenith angle render in Figure 3 suggest.

Both of the images in Figure 5 also show the effects of data striping, perhaps due to faulty cross-calibration of data from adjacent scan mirrors. Unfortunately bands 2, 5, 6, 7, 21, 26, 27, 28, and 33 were all somewhat affected by the striping. Although this poses some challenges in classification, enough bands were salvagable or intact to achieve reasonable results. Table 2 shows the range of bands I chose for initial analysis. The 11 bands I ultimately selected for classification tasks after experimenting with K-means in Section 6 are marked with an asterisk in the table.

### 3 Data and domain of analysis

---

| <b>Band</b> | <b><math>\lambda (\mu m)</math></b> | <b>Justification</b>   |
|-------------|-------------------------------------|--|
| 03*         | .459 – .479                         | Blue band: True color BLUE; sensitive to aerosols.   |
| 10          | .483 – .493                         | Teal/blue: ocean color and general reflectivity.   |
| 04*         | .545 – .565                         | Green: Vegetation, NDSI, and true color GREEN.   |
| 01*         | .620 – .670                         | Near-red: land surface properties, true color RED.   |
| 02*         | .841 – .876                         | NDWI for surface water, and NDVI due to the high reflectance of chlorophyll in the near-infrared range.  |
| 16          | .862 – .877                         | Ocean color and aerosol distinction  |
| 19*         | .916 – .965                         | Partial H <sub>2</sub> O absorption, for column moisture estimates.  |
| 05*         | 1.230 – 1.250                       | Cloud/aerosol optical depth and land surface properties.   |
| 26*         | 1.360 – 1.390                       | Steep H <sub>2</sub> O absorption curve for high cloud reflectance.  |
| 06          | 1.628 – 1.652                       | Snow/ice band: indices of refraction differ between ice and liquid-phase water. Water clouds are reflective and ice clouds strongly absorb.  |
| 07          | 2.106 – 2.155                       | Cloud and aerosol particle size band: small particles are similar in size to $2.2\mu m$ , so they are readily reflected via Mie scattering. Large particles absorb incident light [5]. |
| 20*         | 3.660 – 3.840                       | SWIR “Magic band”: solar reflectance as well as infrared emissions. Useful for a variety of derived products, especially for fire detection.   |
| 21          | 3.929 – 3.989                       | Infrared-biased narrow SWIR for cloud and land surface temperature. Spans the edge of a CO <sub>2</sub> absorption line.   |
| 27          | 6.535 – 6.895                       | High infrared cloud features due to very strong H <sub>2</sub> O absorption.   |
| 28*         | 7.175 – 7.475                       | Mid-level infrared cloud properties due to moderate attenuation by atmospheric water vapor.  |
| 29*         | 8.400 – 8.700                       | Infrared cloud phase and land features, as well as atmospheric column water content from weak vapor absorption. Sensitive to the emissivity of surfaces.                               |
| 31*         | 10.780 – 11.280                     | Clean long-wave window band: very little atmospheric absorption, so the actual temperature of surfaces can be estimated with knowledge of their emissivity.                            |
| 32          | 11.770 – 12.270                     | LWIR window: observed temperatures are slightly sensitive to artificial cooling depending on the altitude of the pixel surface.  |
| 33          | 14.085 – 14.385                     | Dirty LWIR: much stronger attenuation by water vapor makes it easy to characterize column vapor content.   |

\* Starred bands indicate the subset chosen for use in K-means and maximum-likelihood classification. All bands were used for analysis.

Table 2: Band number, spectral response range, and purpose of every MODIS band I used for analysis.

## 4 My custom RGB

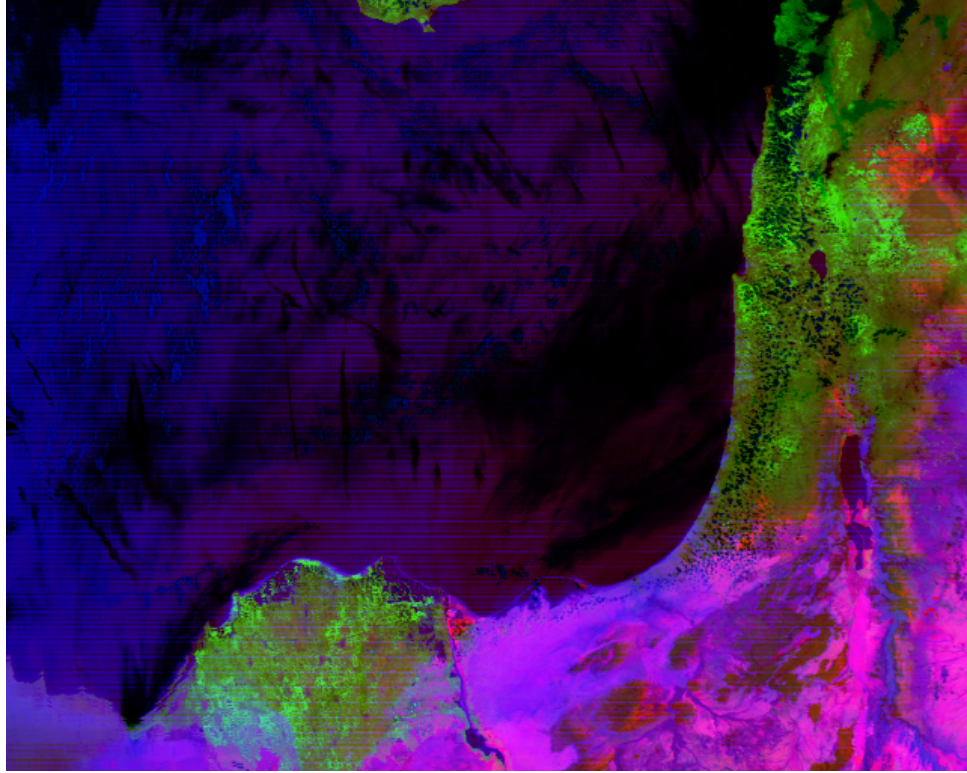


Figure 6: My custom RGB, enhanced to reveal land surface temperature and emissivity, vegetation density, atmospheric vapor content, and to mask thin clouds.

| Custom RGB channels |  | Description   |
|---------------------|--|---|
| RED                 | <pre>gamma(hist(norm(R))) R=T_B(11μm)</pre>            | LWIR window band, histogram-matched to a normal distribution with $\mu = .5$ and $\sigma = .2$ . Saturates cold temperatures to indicate land and sea surface temperature, distinguish land from clouds, and enhance land features.             |
| GREEN               | <pre>gamma(hist(norm(G))) G=NDVI _0^1</pre>            | Subsetted and normalized NDVI, histogram-matched to a normal distribution with $\mu = .3$ and $\sigma = .2$ . Saturates clouds and water near zero and stratifies the brightness histogram over high brightness values in the vegetation range. |
| BLUE                | <pre>gamma(hist(norm(B))) B=T_B(11μm)÷T_B(8.6μm)</pre> | Normalized $11 \div 8.6\mu m$ band ratio, histogram-matched to a normal distribution with $\mu = .5$ and $\sigma = .3$ . Sensitive to land surface emissivity and atmospheric vapor content.  |

Table 3: Custom RGB recipe. Normal distribution values are selected to provide baseline histograms, which can be shifted with gamma enhancement to accentuate the features needed for a specific task.

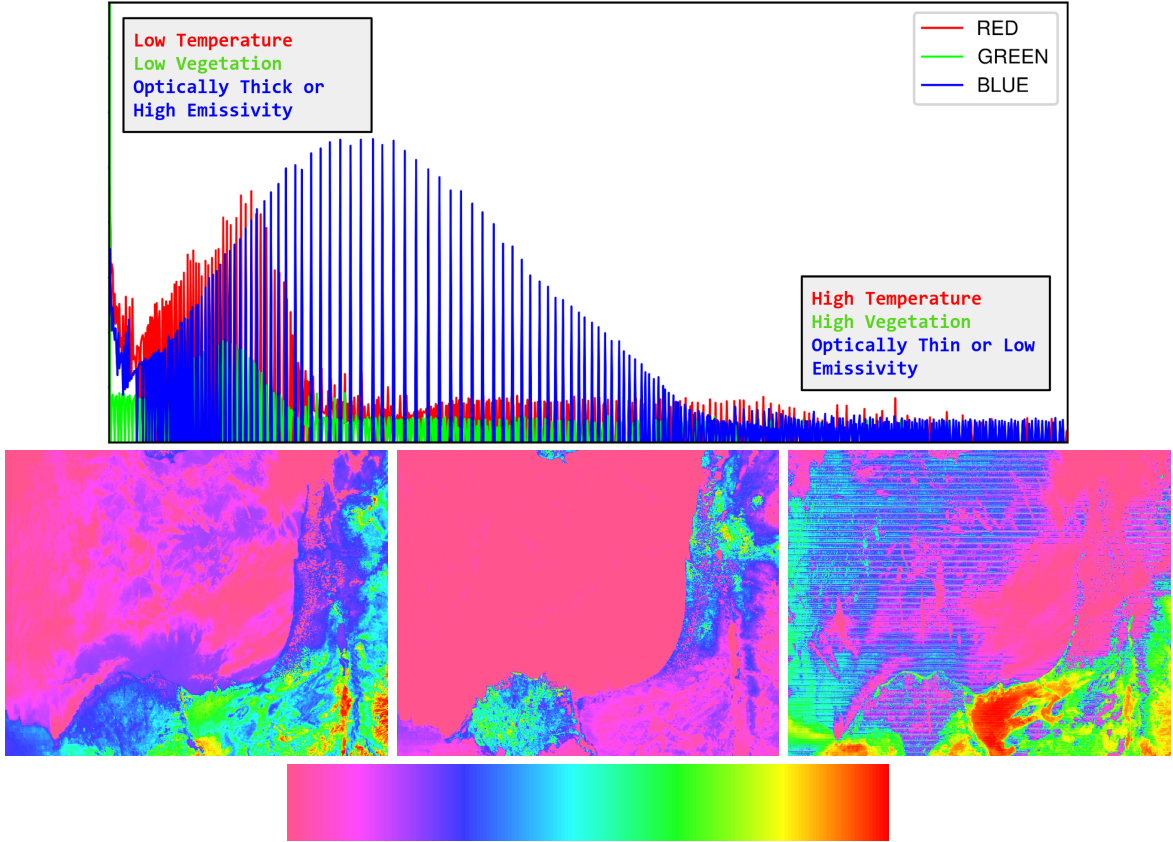


Figure 7: Normalized brightness frequency histogram, and heat map renders of each color component’s scalar array with a colorbar demonstrating the data distribution from minimum (magenta) to maximum (red).

In order to further investigate the features identified in Section 3, I developed an RGB sensitive to vegetation, precipitable water vapor (PWV), land surface and cloud-top temperatures (LST, CTT), and land surface emissivity (LSE). As outlined in Table 3, the RED band is the longwave infrared window, which corresponds directly to LST and CTT, and serves as a reference point for BLUE channel values. The GREEN band is the NDVI with the  $.86\mu m$  and  $.64\mu m$  bands (1 and 2), with high and low values cropped to the  $[0, 1]$  range, then normalized, which saturates barren land, clouds, and water and enhances vegetation density. The BLUE band is the  $11 \div 8.6\mu m$  longwave infrared band ratio, the behavior of which is the most difficult to intuit since bright values correspond to different phenomena on land and in the atmosphere.

On one hand, in the atmosphere, the BLUE band ratio is large where  $8.6\mu m$  band brightness temperatures are suppressed by water vapor as discussed in Section 3. This is apparent at the edges of water clouds, in regions with sub-pixel clouds, and in regions with high PWV. Optically thick (and especially high-altitude) clouds have similar brightness temperatures in both bands, and as such have low ratio values. In clear-sky regions, on the other hand, the BLUE band ratio is dominantly sensitive to LSE. The inverse Planck function `modis.get_modis_data` uses to calculate brightness temperatures from infrared radiance implicitly assumes that the emissivity of incident surfaces is  $\epsilon = 1$ . Since the  $8.4 - 8.7\mu m$  band occupies a spectral range right on the steep low-wavelength edge of the  $T \approx 300K$  blackbody emission curve, it is more sensitive to error in this assumption. Thus low-emissivity surfaces like sand ( $\epsilon \approx .89$ ) appear brighter in the ratio than high-emissivity surfaces like vegetation ( $\epsilon \approx .94$ ).

Both of the phenomena influencing the BLUE band ratio are ultimately the consequence of changes in emissivity among surfaces, as atmospheric layers with a low optical depth equivalently have low emissivity. Nonetheless, my RGB's property that low LSE and high PWV both correlate with high BLUE brightness values can make interpretation challenging. For example in Figure 6, the sandy region Southwest of the Nile Delta appears artificially more blue than the similarly sandy region at the East edge of the delta due to the increased presence of PWV from the moist airmass seen in Figure 5.

I created the custom RGB featured in Figure 6 by adding new scalar recipes for each channel, for example: `subgrid.add_recipe("LWrat", (29, 31), lambda a,b: norm(b/a))`, then an RGB recipe with arguments for each channels using `subgrid.add_rgb_recipe`. Next, I called `guitools.get_normal_rgb` to generate an RGB array with the same shape as my data, which contains normally-distributed scalar values in each 2d channel corresponding to the means and standard deviations specified in Table 3, which are sampled in the [0, 1] range. Then I histogram-matched my custom RGB recipe to the normally-distributed RGB array with `subgrid.histogram_match`, adding the data array to my `subgrid` object with `subgrid.add_rgb_data("CUSTOMhist", rgb)`. Finally, I shifted the brightness histograms to distributions convenient for land-surface analysis by calling `subgrid.get_rgb("CUSTOMhist", choose_gamma=True)`.

Figures 6 and 7 are the results of executing this procedure for a single RGB. The spectral distribution in Figure 7 was generated by calling `subgrid.rgb_histogram_analysis` with the RGB's data label "CUSTOMhist". Each channel heatmap in the figure was created by generating an RGB with `guitools.scal_to_rgb` using custom HSV range parameters, then generating images with `gui_plot.generate_raw_image`.

Low-density vegetation appears brown due to mid-brightness contributions from each channel since partially-vegetated land surfaces are generally warmer, have a lower NDVI, and have a lower total emissivity than heavily vegetated areas. The same logic applies to high and low-vegetation regions since NDVI strongly correlates with surface emissivity as outlined in (Van De Griend, 2007)[6]. After consulting a geographic atlas [7], I realized that the red regions in Jordan and Syria correspond very closely to the Sinai mountain ridge and the Judaean mountains. The geology of this region suggests that these areas mostly consist of exposed and fragmented limestone, which has an emissivity around  $\epsilon = .95$ . The surrounding pink and purple regions are dominantly loamy soil and exposed sandstone, which have emissivities around  $\epsilon = .92$  [7][8][9], hence the contribution from the BLUE channel.

The blue-tinted regions over the Mediterranean on the left of the Figure 6 demonstrate the PWV of the moist air mass over the Mediterranean, as discussed. Optically thick water and dense ice clouds appear black over land and water appear due to their high emissivity and low temperatures in the LWIR window band. The top right of the image features thin cirrus clouds over a vegetated surface, which appear blue/green due to their low emissivity and the diffusion of near-infrared reflectance from vegetation through the cloud. This is an additional example of the interpretation challenge mentioned previously.

## 5 Data thresholding

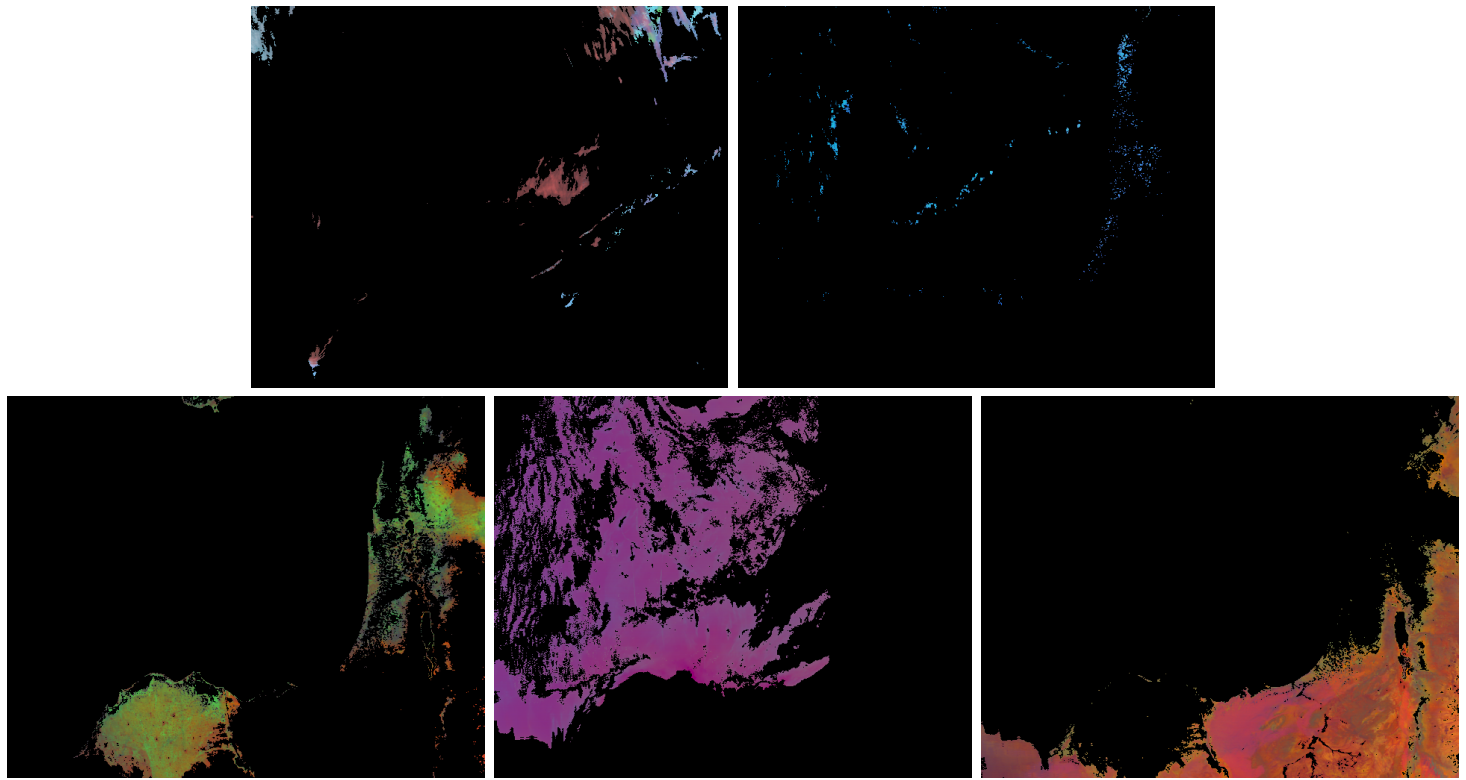


Figure 8: Masks selected by thresholding procedure. Top: ice cloud and water cloud surface classes. Bottom: vegetation, water, and arid surface classes. Unmasked data values are histogram-matched to the primary RGB used to isolate the class.

In order to isolate the 5 surface types I’m analyzing, I manually selected valid reflectance and brightness temperature ranges with `subgrid.get_mask` for a series of bands and RGB recipes. This method launches a GUI interface with a trackbar input form and an image that is rendered with a callback loop depending on the value of the input. For each channel of each RGB in my procedure, I used the trackbar to select a lower and upper bound for the mask. After data ranges for a surface class were determined, I histogram-matched the in-range values to the RGB that best accentuates the surface type using `subgrid.histogram_match`. Figure 8 shows the results, which rule out pixels that were out of bounds for any channel in any image used for thresholding the class.

Histogram-matched surface class masks are useful for interpretation because the histogram matching process spreads out brightness values of RGB channels with high variance for data values in the class. For example, the vegetation mask was histogram-matched to my custom RGB. There are a wide range of plant densities visible in this mask due to the variability in the RED (LWIR) and GREEN (NDVI) channels of my custom RGB. The water mask, which was also matched to my RGB, features a bright region just Northeast of the Nile Delta, which corresponds to warmer regions in the RED (LWIR) channel from a relative lack of sub-pixel clouds and atmospheric moisture, as suggested by the  $7.3\mu\text{m}$  channel rendering in Figure 5, and the relatively high temperature and low emissivity in this region indicated by Figure 7’s RED and BLUE channels.

## Thresholding methodology

1. The **ice cloud** class is selected with upper and lower bounds on each channel of the daytime cloud-phase RGB, which includes the  $1.38\mu m$  cirrus band for middle and low-cloud masking as well as the  $1.64\mu m$  cloud-phase band to rule out water clouds.
2. The **water cloud** mask is selected by masking ice clouds with the daytime cloud-phase RGB, and land surfaces with my custom RGB.
3. The **arid land** mask is selected using my custom RGB, which was specifically enhanced to accentuate land features and vegetation as discussed in Section 4.
4. The **vegetation** mask is also selected with my custom RGB, using a different gamma enhancement after histogram-matching which is selected manually to better expose vegetation. I used my own discretion to set boundaries where vegetation became too sparse.
5. The **water** class is the most difficult to isolate due to the abundance of PWV and sub-pixel clouds in my case. Optically thick clouds and most land are masked with my custom RGB, then coastlines are masked with the  $8.6 - 2.1\mu m$  NIR water index (NDWI). Finally, all prior masks are negated from the water mask.

|                        | Ice Cloud | Water Cloud | Vegetation | Water   | Arid   |
|------------------------|-----------|-------------|------------|---------|--------|
| Pixel Count            | 10,094    | 2,227       | 36,614     | 96,730  | 68,922 |
| Area ( $\text{km}^2$ ) | 14,426    | 3,221       | 48,431     | 181,319 | 85,435 |

Table 4: Area and quantity of thresholded pixel classes.

Table 4 shows the number of pixels and approximate surface area of each of the classes derived from thresholding. Areas were calculated for each surface type by passing the 2d boolean array returned by `subgrid.get_mask` to the `subgrid.area` method, which returns the sum of the surface areas of unmasked pixels by calculating the pixelwise panoramic distortion with the viewing zenith angle array (`subgrid.data("vza")`). This table makes clear that water and arid land dominate the region, followed by vegetated land surfaces.

Ice clouds and water clouds are under-represented because I intentionally chose restrictive thresholds for these classes. Clouds in general were difficult to threshold due to the scarcity of vapor bands uncorrupted by striping, the wide range of PWV values in my region, and the presence of mixed-phase clouds over the Mediterranean. For example, note the light blue mid-level water-phase clouds present on the right side of the ice cloud mask in Figure 8. These inhabit a region with low precipitable water vapor and a very thin cirrus layer, and as such weren't masked with a lower bound on LWIR brightness temperature or the  $1.37\mu m$  cirrus band. Since I will sub-sample my thresholded classes to use as training samples for MLC, I wanted to leave as little ambiguity as possible in each class' spectral signature.

### Thresholded surface classes: spectral response and error

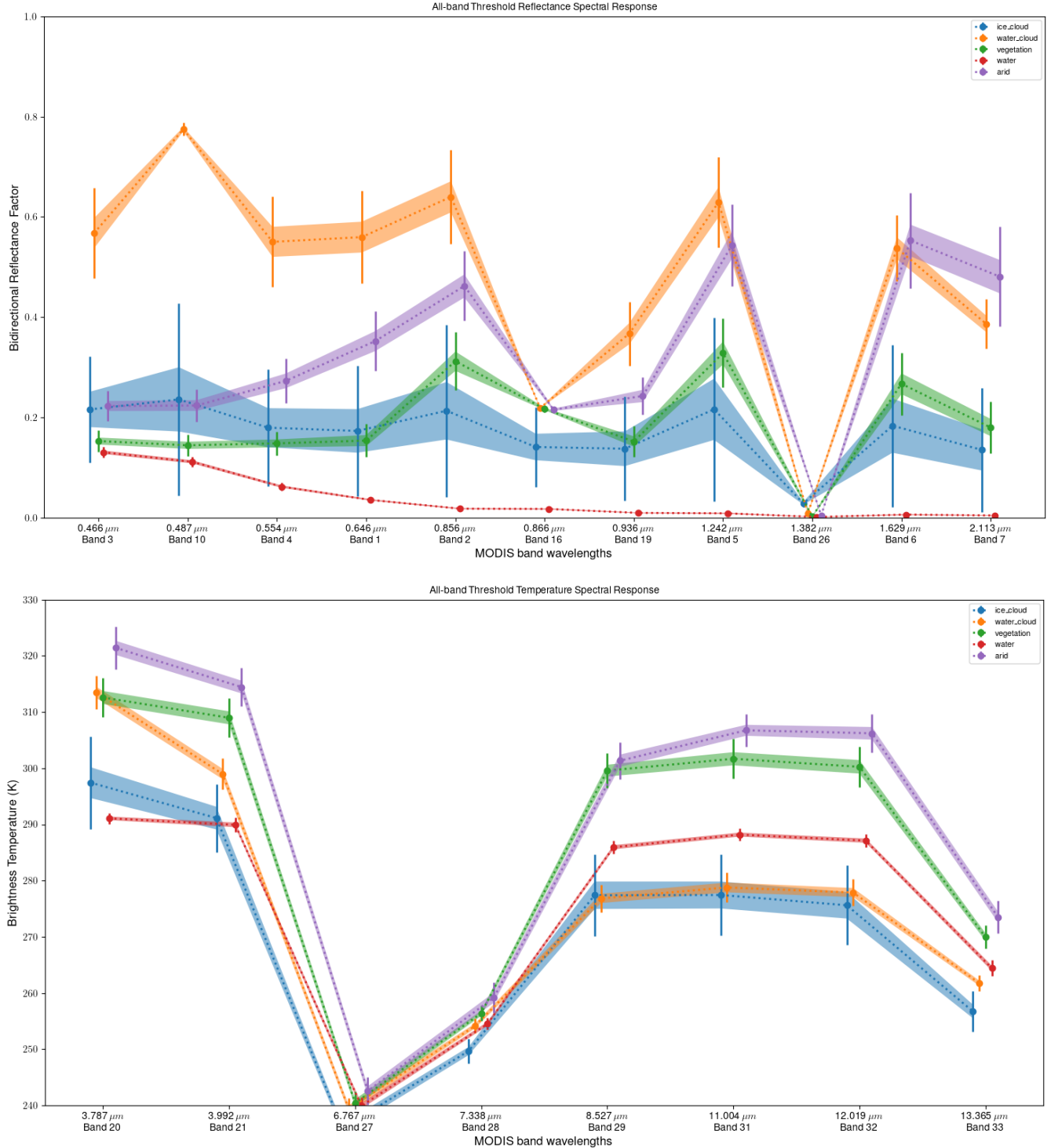


Figure 9: Reflective and thermal spectral response of each threshold-derived surface class. Each data point is the mean value of the class at that wavelength with  $1 - \sigma$  error bars and  $\frac{1}{3} - \sigma$  shaded regions. These plots were generated with the surface class masks from the thresholding procedure using `subgrid.spectral_analysis`, which is a wrapper on the `geo_plot.stats_1d` function.

| $\lambda$   | $\mu$ | $\sigma$ | Reflectance Covariance ( $\times 10^4$ ) |       |       |       |       |       |      |  |
|-------------|-------|----------|--|-------|-------|-------|-------|-------|------|--|
| Ice Cloud   |       |          |  |       |       |       |       |       |      |  |
| 0.466       | 0.216 | 0.105    | 111.3                                    | 118.5 | 125.2 | 138.0 | 88.5  | 135.7 | 0.5  |  |
| 0.554       | 0.180 | 0.117    | 118.5                                    | 136.2 | 150.1 | 180.7 | 112.2 | 181.6 | 0.6  |  |
| 0.646       | 0.173 | 0.130    | 125.2                                    | 150.1 | 169.8 | 211.0 | 129.4 | 215.2 | 0.6  |  |
| 0.856       | 0.214 | 0.172    | 138.0                                    | 180.7 | 211.0 | 295.0 | 176.3 | 309.1 | 1.1  |  |
| 0.936       | 0.138 | 0.104    | 88.5                                     | 112.2 | 129.4 | 176.3 | 107.7 | 184.0 | 0.9  |  |
| 1.242       | 0.216 | 0.183    | 135.7                                    | 181.6 | 215.2 | 309.1 | 184.0 | 335.2 | 1.2  |  |
| 1.382       | 0.029 | 0.008    | 0.5                                      | 0.6   | 0.6   | 1.1   | 0.9   | 1.2   | 0.6  |  |
| Water Cloud |       |          |  |       |       |       |       |       |      |  |
| 0.466       | 0.560 | 0.092    | 84.9                                     | 81.5  | 81.2  | 82.5  | 68.0  | 47.9  | 0.0  |  |
| 0.554       | 0.640 | 0.093    | 81.5                                     | 86.7  | 75.1  | 78.8  | 76.1  | 54.3  | 0.9  |  |
| 0.646       | 0.568 | 0.090    | 81.2                                     | 75.1  | 81.3  | 80.1  | 61.9  | 41.8  | -0.6 |  |
| 0.856       | 0.550 | 0.090    | 82.5                                     | 78.8  | 80.1  | 80.7  | 65.4  | 45.8  | -0.1 |  |
| 0.936       | 0.629 | 0.090    | 68.0                                     | 76.1  | 61.9  | 65.4  | 81.0  | 49.5  | 1.1  |  |
| 1.242       | 0.367 | 0.063    | 47.9                                     | 54.3  | 41.8  | 45.8  | 49.5  | 40.2  | 1.7  |  |
| 1.382       | 0.009 | 0.006    | 0.0                                      | 0.9   | -0.6  | -0.1  | 1.1   | 1.7   | 0.3  |  |
| Vegetation  |       |          |  |       |       |       |       |       |      |  |
| 0.466       | 0.154 | 0.033    | 10.9                                     | 8.4   | 4.6   | 7.0   | 14.3  | 5.3   | 0.4  |  |
| 0.554       | 0.312 | 0.058    | 8.4                                      | 33.5  | 4.4   | 7.2   | 36.5  | 15.0  | 0.1  |  |
| 0.646       | 0.153 | 0.021    | 4.6                                      | 4.4   | 4.4   | 4.5   | 6.3   | 0.7   | 0.0  |  |
| 0.856       | 0.149 | 0.024    | 7.0                                      | 7.2   | 4.5   | 5.6   | 10.5  | 3.1   | 0.1  |  |
| 0.936       | 0.329 | 0.068    | 14.3                                     | 36.5  | 6.3   | 10.5  | 46.8  | 18.0  | 0.4  |  |
| 1.242       | 0.152 | 0.031    | 5.3                                      | 15.0  | 0.7   | 3.1   | 18.0  | 9.6   | 0.4  |  |
| 1.382       | 0.003 | 0.003    | 0.4                                      | 0.1   | 0.0   | 0.1   | 0.4   | 0.4   | 0.1  |  |
| Water       |       |          |  |       |       |       |       |       |      |  |
| 0.466       | 0.036 | 0.005    | 0.2                                      | 0.1   | 0.3   | 0.3   | 0.1   | 0.1   | 0.0  |  |
| 0.554       | 0.018 | 0.004    | 0.1                                      | 0.1   | 0.2   | 0.2   | 0.1   | 0.1   | 0.0  |  |
| 0.646       | 0.131 | 0.010    | 0.3                                      | 0.2   | 1.1   | 0.5   | 0.1   | 0.0   | -0.0 |  |
| 0.856       | 0.062 | 0.007    | 0.3                                      | 0.2   | 0.5   | 0.5   | 0.1   | 0.1   | 0.0  |  |
| 0.936       | 0.009 | 0.004    | 0.1                                      | 0.1   | 0.1   | 0.1   | 0.2   | 0.1   | 0.0  |  |
| 1.242       | 0.010 | 0.002    | 0.1                                      | 0.1   | 0.0   | 0.1   | 0.1   | 0.1   | 0.0  |  |
| 1.382       | 0.002 | 0.002    | 0.0                                      | 0.0   | -0.0  | 0.0   | 0.0   | 0.0   | 0.0  |  |
| Arid        |       |          |  |       |       |       |       |       |      |  |
| 0.466       | 0.352 | 0.060    | 35.6                                     | 39.7  | 15.3  | 25.2  | 44.5  | 14.7  | -0.3 |  |
| 0.554       | 0.462 | 0.069    | 39.7                                     | 47.8  | 17.2  | 28.0  | 53.6  | 16.5  | -0.5 |  |
| 0.646       | 0.223 | 0.030    | 15.3                                     | 17.2  | 8.8   | 12.4  | 18.9  | 4.7   | -0.3 |  |
| 0.856       | 0.273 | 0.044    | 25.2                                     | 28.0  | 12.4  | 19.1  | 31.1  | 9.6   | -0.3 |  |
| 0.936       | 0.544 | 0.082    | 44.5                                     | 53.6  | 18.9  | 31.1  | 67.0  | 20.2  | -0.4 |  |
| 1.242       | 0.243 | 0.037    | 14.7                                     | 16.5  | 4.7   | 9.6   | 20.2  | 13.5  | 0.4  |  |
| 1.382       | 0.005 | 0.003    | -0.3                                     | -0.5  | -0.3  | -0.3  | -0.4  | 0.4   | 0.1  |  |

Table 5: Thresholded surface class means, standard deviations, and covariance matrices for each of the MODIS reflectance bands selected for classification.

| $\lambda$   | $\mu$ | $\sigma$ | Brightness Temp. Covariance ( $\times 10^2$ ) |       |        |        |
|-------------|-------|----------|---|-------|--------|--------|
| Ice Cloud   |       |          |   |       |        |        |
| 3.79        | 297.5 | 8.23     | 6771.7  | 808.8 | 332.1  | 711.5  |
| 7.34        | 249.7 | 2.19     | 808.8   | 479.0 | 317.0  | 475.6  |
| 8.53        | 277.4 | 7.32     | 332.1   | 317.0 | 5356.4 | 5191.0 |
| 11.00       | 277.4 | 7.19     | 711.5   | 475.6 | 5191.0 | 5163.8 |
| Water Cloud |       |          |   |       |        |        |
| 3.79        | 313.5 | 2.98     | 888.6   | 176.3 | 244.8  | 270.8  |
| 7.34        | 254.1 | 1.28     | 176.3   | 164.8 | 195.4  | 233.4  |
| 8.53        | 276.8 | 2.47     | 244.8   | 195.4 | 612.1  | 627.3  |
| 11.00       | 278.8 | 2.61     | 270.8   | 233.4 | 627.3  | 683.9  |
| Vegetation  |       |          |   |       |        |        |
| 3.79        | 312.6 | 3.47     | 1201.7  | 212.7 | 867.3  | 1000.8 |
| 7.34        | 256.4 | 1.36     | 212.7   | 185.1 | 213.2  | 273.4  |
| 8.53        | 299.6 | 3.14     | 867.3   | 213.2 | 983.6  | 1063.9 |
| 11.00       | 301.7 | 3.51     | 1000.8  | 273.4 | 1063.9 | 1229.4 |
| Water       |       |          |   |       |        |        |
| 3.79        | 291.1 | 0.97     | 94.4  | 56.1  | 87.1   | 76.3   |
| 7.34        | 254.5 | 1.03     | 56.1  | 106.4 | 79.5   | 71.0   |
| 8.53        | 285.9 | 1.12     | 87.1  | 79.5  | 126.1  | 117.3  |
| 11.00       | 288.2 | 1.09     | 76.3  | 71.0  | 117.3  | 119.8  |
| Arid        |       |          |   |       |        |        |
| 3.79        | 321.4 | 3.77     | 1418.6  | 350.3 | -164.7 | 832.2  |
| 7.34        | 259.2 | 2.69     | 350.3   | 726.0 | 330.6  | 475.0  |
| 8.53        | 301.3 | 3.24     | -164.7  | 330.6 | 1047.7 | 357.2  |
| 11.00       | 306.7 | 2.92     | 832.2   | 475.0 | 357.2  | 855.3  |

Table 6: Brightness temperature means, standard deviations, and covariance matrices for each class identified by manual thresholding.

### Thresholded surface class analysis

Figure 9 shows the standard deviation and mean spectral response of each of my surface classes, using all the bands in Table 2. The reflectance of ice clouds in the top image has the largest standard deviation of all surface classes due to the aforementioned presence of water-phase clouds and the wide range in cirrus optical depth. Nonetheless, it's clear that the slope of mean ice cloud reflectance is less affected by absorption lines at  $.856\mu m$ ,  $.936\mu m$ , and  $1.382\mu m$  due to the relative scarcity of water vapor above the cirrus clouds' altitude. Table 5 indicates that the reflectance curve of the vegetation class has a much lower standard deviation of around .03 in window bands. The hallmark jump in NIR reflectance over vegetation is readily apparent in its spectral response curve in Figure 9. The reflectance spectral response of water is most consistent, and characteristically peaks in the blue range, decreasing steeply to almost zero into the NIR range. As their bright white color suggests, clouds are by far the most reflective class in the visible range. The relatively high reflectivity of water clouds in the  $1.629\mu m$  cloud phase band isn't well-represented by the thresholded samples because most of the cirrus clouds in my image are extremely thin, as mentioned in Section 3. I chose not to use the  $1.629\mu m$  band in classification because of these challenges, which means I will rely on infrared and  $1.37\mu m$  NIR absorption bands alone for cirrus identification.

## 6 K-means classification

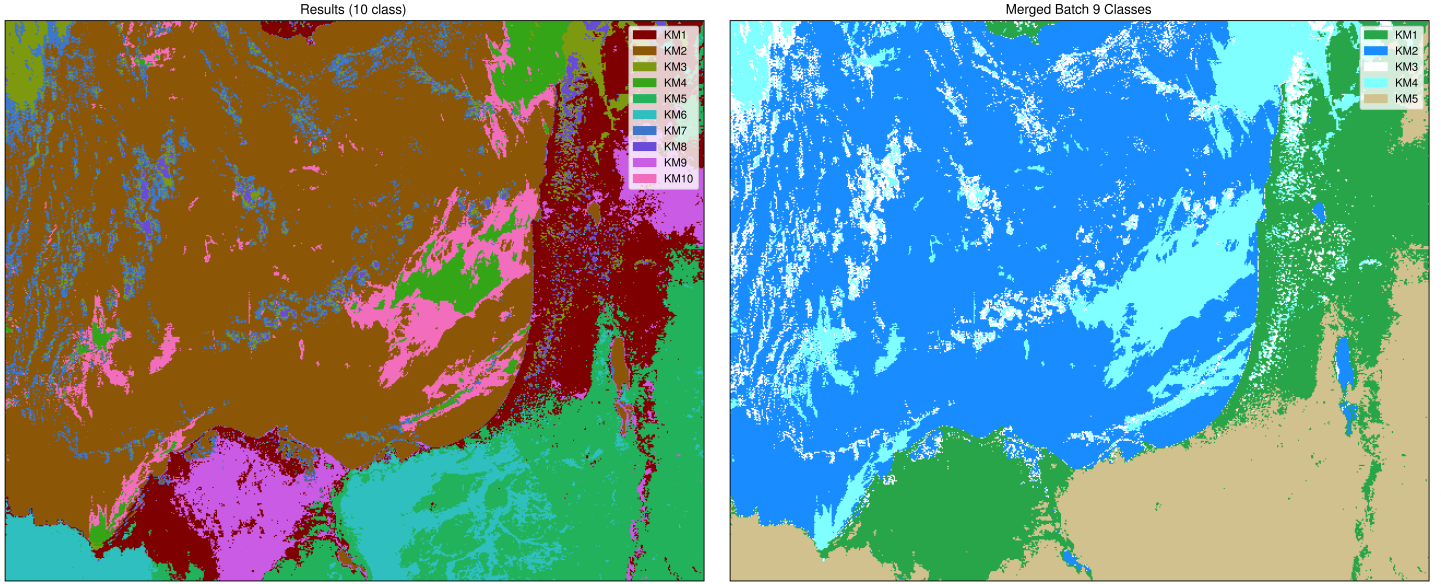


Figure 10: Final set of K-means results, which were trained on the 11 starred bands in Table 2. I determined that 10 classes was an appropriate number of categories to capture a variety of features without finding mean vectors that are too close together given the bands I selected. These 10 classes were subsequently manually merged to reflect the 5 surface classes I chose for analysis.

|                         | KM1<br>(vegetation) | KM2<br>(water) | KM3<br>(water cloud) | KM4<br>(ice cloud) | KM5<br>(arid) |
|-------------------------|---------------------|----------------|----------------------|--------------------|---------------|
| Pixel Count             | 57,991              | 149,596        | 20,064               | 37,428             | 62,601        |
| Area (km <sup>2</sup> ) | 71,817              | 277,355        | 42,338               | 58,480             | 78,696        |

Table 7: Area and quantity of K-means pixel classes.

In order to determine the ideal set of MODIS bands to use for MLC, I performed unsupervised K-means classification on combinations of the channels in Table 2. K-means (ie migrating means) classification can be executed on any set of bands or scalar recipes with `subgrid.get_kmeans`. Although classification may have been aided by using scalar band composites like NDVI as inputs, I chose to use only the bands' TOA reflectances (BRDF) or estimated brightness temperatures as inputs to each of the classification strategies.

In previous assignments, I used an optional conditional statement my k-means implementation (`classify.k_means`) to automatically merge classes with nearby means. After many K-means runs with a variety of band configurations and class counts, I determined that surface classes were most consistently separated by initializing K-means with 14 classes, and setting thresholds to automatically merge down to 9-10 classes. Several combinations of bands produced results similar to those in Figure 10, but the combination least impacted by atmospheric moisture and data striping are the bands featured in Figure 11 and Tables 8 and 9. These are also the starred bands in Table 2, and the subset used for MLC.

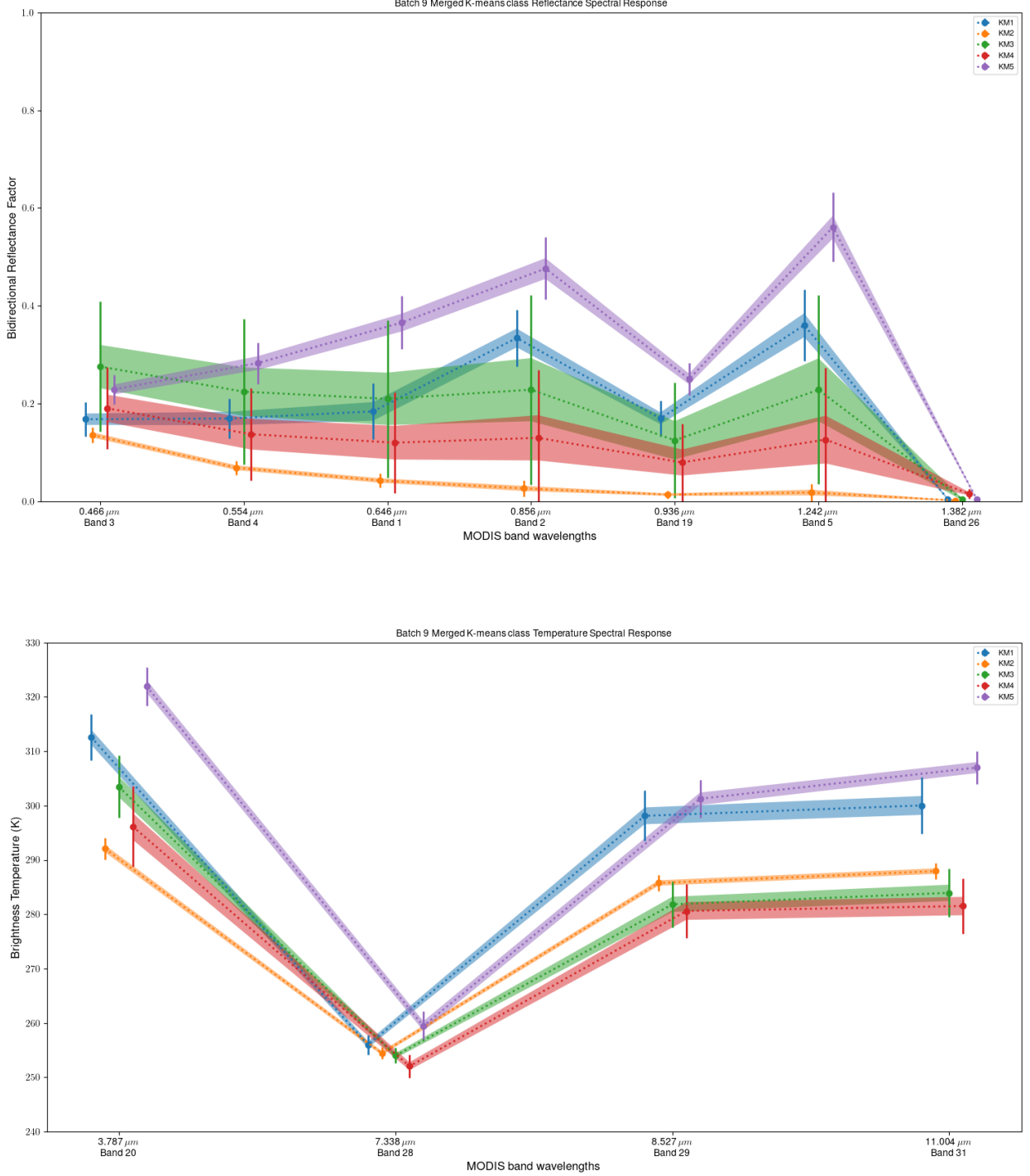


Figure 11: Mean spectral response of K-means classes for each of the bands used as classification inputs, with  $1 - \sigma$  error bars and  $\frac{1}{3} - \sigma$  shaded regions. Top: reflectance bands, bottom: emissive bands. The bands with the highest standard deviation are KM3, which is green in the spectral plots and corresponds to water clouds, and KM4, which is red in the spectral plots and corresponds to ice clouds. Note the steep slope of the  $8.5\mu\text{m}$  to  $11\mu\text{m}$  infrared brightness temperature of KM5 (purple, arid), which corresponds to the differences in land surface emissivity mentioned in Section 4.

| $\lambda$         | $\mu$ | $\sigma$ | Reflectance Covariance ( $\times 10^4$ ) |       |       |       |       |       |      |  |
|-------------------|-------|----------|--|-------|-------|-------|-------|-------|------|--|
| KM1 (Vegetation)  |       |          |  |       |       |       |       |       |      |  |
| 0.466             | 0.168 | 0.035    | 12.3                                     | 13.4  | 15.3  | 11.1  | 5.7   | 14.8  | 0.5  |  |
| 0.554             | 0.170 | 0.041    | 13.4                                     | 16.8  | 22.0  | 15.7  | 9.4   | 22.0  | 0.7  |  |
| 0.646             | 0.184 | 0.057    | 15.3                                     | 22.0  | 32.7  | 20.4  | 14.1  | 31.3  | 1.2  |  |
| 0.856             | 0.334 | 0.058    | 11.1                                     | 15.7  | 20.4  | 33.3  | 17.6  | 39.2  | 0.7  |  |
| 0.936             | 0.170 | 0.036    | 5.7                                      | 9.4   | 14.1  | 17.6  | 13.3  | 22.8  | 1.0  |  |
| 1.242             | 0.361 | 0.074    | 14.8                                     | 22.0  | 31.3  | 39.2  | 22.8  | 54.1  | 1.3  |  |
| 1.382             | 0.005 | 0.005    | 0.5                                      | 0.7   | 1.2   | 0.7   | 1.0   | 1.3   | 0.3  |  |
| KM2 (Water)       |       |          |  |       |       |       |       |       |      |  |
| 0.466             | 0.043 | 0.014    | 1.9                                      | 2.1   | 1.8   | 1.9   | 2.3   | 1.0   | 0.0  |  |
| 0.554             | 0.027 | 0.016    | 2.1                                      | 2.5   | 1.8   | 2.0   | 2.7   | 1.2   | 0.0  |  |
| 0.646             | 0.136 | 0.016    | 1.8                                      | 1.8   | 2.6   | 1.9   | 1.9   | 0.8   | -0.1 |  |
| 0.856             | 0.069 | 0.015    | 1.9                                      | 2.0   | 1.9   | 2.1   | 2.2   | 0.9   | 0.0  |  |
| 0.936             | 0.018 | 0.018    | 2.3                                      | 2.7   | 1.9   | 2.2   | 3.1   | 1.3   | 0.0  |  |
| 1.242             | 0.014 | 0.008    | 1.0                                      | 1.2   | 0.8   | 0.9   | 1.3   | 0.6   | 0.0  |  |
| 1.382             | 0.002 | 0.002    | 0.0                                      | 0.0   | -0.1  | 0.0   | 0.0   | 0.0   | 0.1  |  |
| KM3 (Water Cloud) |       |          |  |       |       |       |       |       |      |  |
| 0.466             | 0.210 | 0.161    | 257.8                                    | 308.1 | 210.7 | 238.6 | 301.9 | 185.3 | 5.3  |  |
| 0.554             | 0.229 | 0.194    | 308.1                                    | 375.5 | 249.0 | 284.6 | 370.1 | 226.1 | 6.7  |  |
| 0.646             | 0.276 | 0.133    | 210.7                                    | 249.0 | 175.6 | 195.9 | 243.7 | 149.3 | 4.0  |  |
| 0.856             | 0.225 | 0.149    | 238.6                                    | 284.6 | 195.9 | 221.2 | 278.7 | 171.0 | 4.8  |  |
| 0.936             | 0.228 | 0.193    | 301.9                                    | 370.1 | 243.7 | 278.7 | 372.0 | 223.3 | 6.7  |  |
| 1.242             | 0.125 | 0.118    | 185.3                                    | 226.1 | 149.3 | 171.0 | 223.3 | 138.1 | 4.5  |  |
| 1.382             | 0.004 | 0.006    | 5.3                                      | 6.7   | 4.0   | 4.8   | 6.7   | 4.5   | 0.3  |  |
| KM4 (Ice Cloud)   |       |          |  |       |       |       |       |       |      |  |
| 0.466             | 0.120 | 0.103    | 106.5                                    | 138.2 | 82.6  | 96.6  | 143.1 | 78.3  | -0.1 |  |
| 0.554             | 0.130 | 0.139    | 138.2                                    | 192.6 | 101.1 | 123.8 | 201.5 | 109.2 | 0.7  |  |
| 0.646             | 0.191 | 0.084    | 82.6                                     | 101.1 | 70.4  | 77.2  | 104.5 | 56.7  | -0.8 |  |
| 0.856             | 0.138 | 0.094    | 96.6                                     | 123.8 | 77.2  | 88.6  | 128.0 | 69.9  | -0.3 |  |
| 0.936             | 0.127 | 0.147    | 143.1                                    | 201.5 | 104.5 | 128.0 | 215.0 | 114.3 | 0.8  |  |
| 1.242             | 0.080 | 0.080    | 78.3                                     | 109.2 | 56.7  | 69.9  | 114.3 | 63.4  | 1.2  |  |
| 1.382             | 0.016 | 0.010    | -0.1                                     | 0.7   | -0.8  | -0.3  | 0.8   | 1.2   | 0.9  |  |
| KM5 (Arid)        |       |          |  |       |       |       |       |       |      |  |
| 0.466             | 0.366 | 0.055    | 29.8                                     | 33.7  | 13.9  | 22.0  | 34.6  | 10.5  | -0.3 |  |
| 0.554             | 0.476 | 0.064    | 33.7                                     | 40.6  | 15.9  | 24.9  | 42.0  | 11.5  | -0.5 |  |
| 0.646             | 0.229 | 0.030    | 13.9                                     | 15.9  | 9.2   | 12.0  | 15.9  | 3.8   | -0.3 |  |
| 0.856             | 0.283 | 0.042    | 22.0                                     | 24.9  | 12.0  | 17.8  | 25.1  | 7.5   | -0.3 |  |
| 0.936             | 0.561 | 0.071    | 34.6                                     | 42.0  | 15.9  | 25.1  | 49.8  | 12.8  | -0.5 |  |
| 1.242             | 0.251 | 0.033    | 10.5                                     | 11.5  | 3.8   | 7.5   | 12.8  | 10.9  | 0.4  |  |
| 1.382             | 0.005 | 0.003    | -0.3                                     | -0.5  | -0.3  | -0.3  | -0.5  | 0.4   | 0.1  |  |

Table 8: Mean class values and standard deviations for each reflectance band and covariance matrices for each surface type identified by K-means classification.

| $\lambda$         | $\mu$ | $\sigma$ | Brightness | Temp. | Covariance ( $\times 10^2$ ) |         |
|-------------------|-------|----------|------------|-------|------------------------------|---------|
| KM1 (Vegetation)  |       |          |            |       |                              |         |
| 3.79              | 312.6 | 4.23     | 1793.4     | 395.7 | 1422.1                       | 1661.1  |
| 7.34              | 256.0 | 1.79     | 395.7      | 319.0 | 470.3                        | 586.3   |
| 8.53              | 298.1 | 4.63     | 1422.1     | 470.3 | 2146.3                       | 2363.0  |
| 11.00             | 300.0 | 5.20     | 1661.1     | 586.3 | 2363.0                       | 2704.1  |
| KM2 (Water)       |       |          |            |       |                              |         |
| 3.79              | 292.1 | 2.01     | 404.0      | 60.5  | 94.8                         | 83.7    |
| 7.34              | 254.5 | 1.12     | 60.5       | 126.4 | 114.8                        | 107.6   |
| 8.53              | 285.8 | 1.51     | 94.8       | 114.8 | 228.1                        | 223.0   |
| 11.00             | 287.9 | 1.53     | 83.7       | 107.6 | 223.0                        | 233.9   |
| KM3 (Water Cloud) |       |          |            |       |                              |         |
| 3.79              | 303.5 | 5.72     | 3276.2     | 110.1 | -959.3                       | -1048.7 |
| 7.34              | 254.0 | 1.39     | 110.1      | 193.1 | 311.5                        | 332.5   |
| 8.53              | 281.8 | 4.22     | -959.3     | 311.5 | 1777.6                       | 1873.9  |
| 11.00             | 284.0 | 4.48     | -1048.7    | 332.5 | 1873.9                       | 2009.4  |
| KM4 (Ice Cloud)   |       |          |            |       |                              |         |
| 3.79              | 296.2 | 7.35     | 5405.7     | 478.3 | -1124.8                      | -932.1  |
| 7.34              | 252.1 | 2.17     | 478.3      | 469.9 | 459.4                        | 596.8   |
| 8.53              | 280.6 | 4.90     | -1124.8    | 459.4 | 2404.9                       | 2440.2  |
| 11.00             | 281.5 | 5.06     | -932.1     | 596.8 | 2440.2                       | 2563.5  |
| KM5 (Arid)        |       |          |            |       |                              |         |
| 3.79              | 322.0 | 3.55     | 1257.1     | 272.8 | -185.0                       | 741.5   |
| 7.34              | 259.4 | 2.66     | 272.8      | 709.5 | 412.8                        | 470.0   |
| 8.53              | 301.3 | 3.45     | -185.0     | 412.8 | 1192.0                       | 460.9   |
| 11.00             | 307.0 | 3.03     | 741.5      | 470.0 | 460.9                        | 918.3   |

Table 9: Mean class values and standard deviations for each emissive band and covariance matrices for each surface type identified by K-means classification.

### K-means results analysis

The mean value and variance of the  $1.382\mu m$  cirrus band is highest in the Ice Cloud class (per the bottom right value in the covariance matrices) with  $\sigma^2 = 9 \times 10^{-4}$ , which is appropriate since values for other classes are mostly attenuated by atmospheric water vapor in the absorption band. The vegetation and water classes also have relatively high mean values of  $\mu = .005$  in the cirrus band because of the lack of water vapor in the regions East and Southeast of the moist Mediterranean airmass.

The water cloud class (KM3) has the highest variance of all classes in all reflectance bands, and of all classes in all emissive bands except for the ice cloud class (KM4). This is a symptom of the same challenges that made it difficult to select thresholds for water in Section 5. Despite these challenges, K-means was much bolder than my thresholds in classifying thin ice clouds over land and water. With all the band combinations I tried, the cirrus band ( $1.382\mu m$ ) and the mid-level water vapor band ( $7.34\mu m$ ) were least affected by data striping and had the lowest variance within the ice cloud class, so these likely contributed most strongly to ice cloud designation.

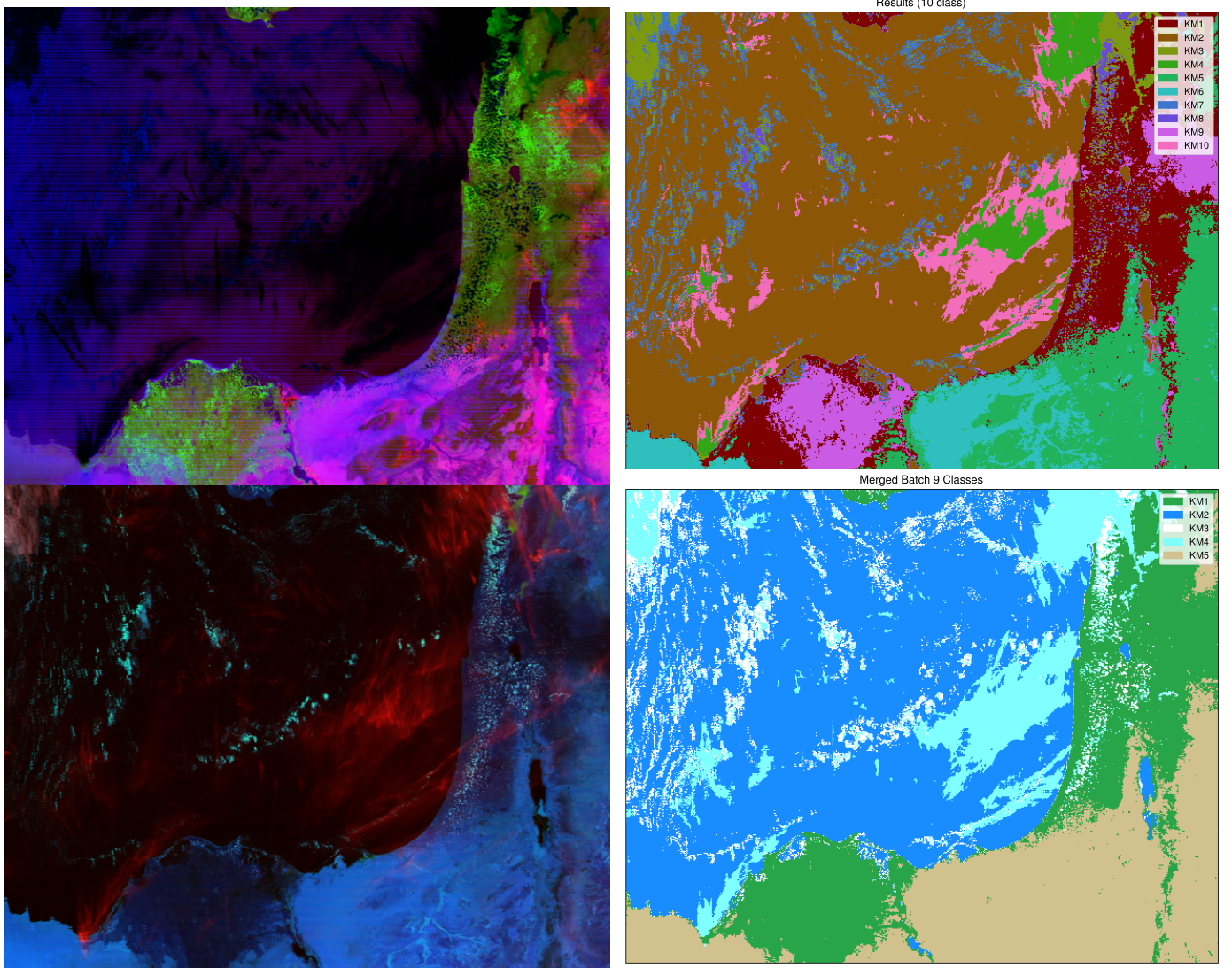


Figure 12: Top: my custom RGB compared to the 10-class K-means results I merged to represent my 5 classes. Bottom: daytime cloud phase RGB compared to the 5 manually-merged K-means classes. The K-means class maps were generated with `geo_plot.plot_classes`.

Figure 12 includes a day-cloud phase RGB compared to my K-means results. Both cloud types and all 3 surface types are well-characterized by their merged K-means classes. Since my region is covered by cirrus clouds with a wide range of optical depths, and a smattering of small and sub-pixel water clouds, I needed to manually merge 3 separate K-means classes for thick cirrus (dark and light green), thin cirrus (pink), and 2 class for water clouds (purple and dull blue). I believe the cirrus means were separated due to the KM4 class' high variance in the  $.936\mu m$  vapor absorption band, which is sensitive to the cirrus clouds' optical depth. Similarly, the water cloud class was probably separated into multiple means due to its high variance in the  $.936\mu m$  channel, as well as  $3.79\mu m$  brightness temperatures (and reflectance) due to the wide range of optical depth and cloud top temperatures.

Compared to my custom RGB in Figure 12, it's also clear that the 10-class K-means run separated the arid surface into the low-emissivity sandy regions (KM6, cyan) and

## 7 Samples from thresholded classes

---

high-emissivity exposed and loamy regions (KM5, pastel green) identified in Section 4, which I merged into my more restrictive “arid” surface class. Likewise, the 10-class K-means run identified sparse vegetation (KM9, magenta) and dense vegetation (KM1, red) separately.

|            | Ice Cloud | Water Cloud | Vegetation | Water | Arid  | Cons. Acc. |
|------------|-----------|-------------|------------|-------|-------|------------|
| KM1        | 766       | 0           | 35940      | 0     | 8023  | 0.804      |
| KM2        | 0         | 0           | 195        | 96348 | 79    | 0.997      |
| KM3        | 518       | 2213        | 326        | 0     | 5     | 0.723      |
| KM4        | 8736      | 12          | 0          | 382   | 0     | 0.957      |
| KM5        | 74        | 2           | 153        | 0     | 60815 | 0.996      |
| Prod. Acc. | 0.865     | 0.994       | 0.982      | 0.996 | 0.882 |            |

Table 10: Confusion matrix comparing my threshold-derived surface classes to the K-means results. The lowest consumer accuracies are in the KM1 (vegetation) and KM3 (water cloud) classes, which were most commonly confused with arid and ice cloud classes, respectively. This is because I chose restrictive thresholds for vegetation, and because my ice cloud thresholds erroneously included some water clouds (See Figure 8), which K-means successfully avoided.

## 7 Samples from thresholded classes

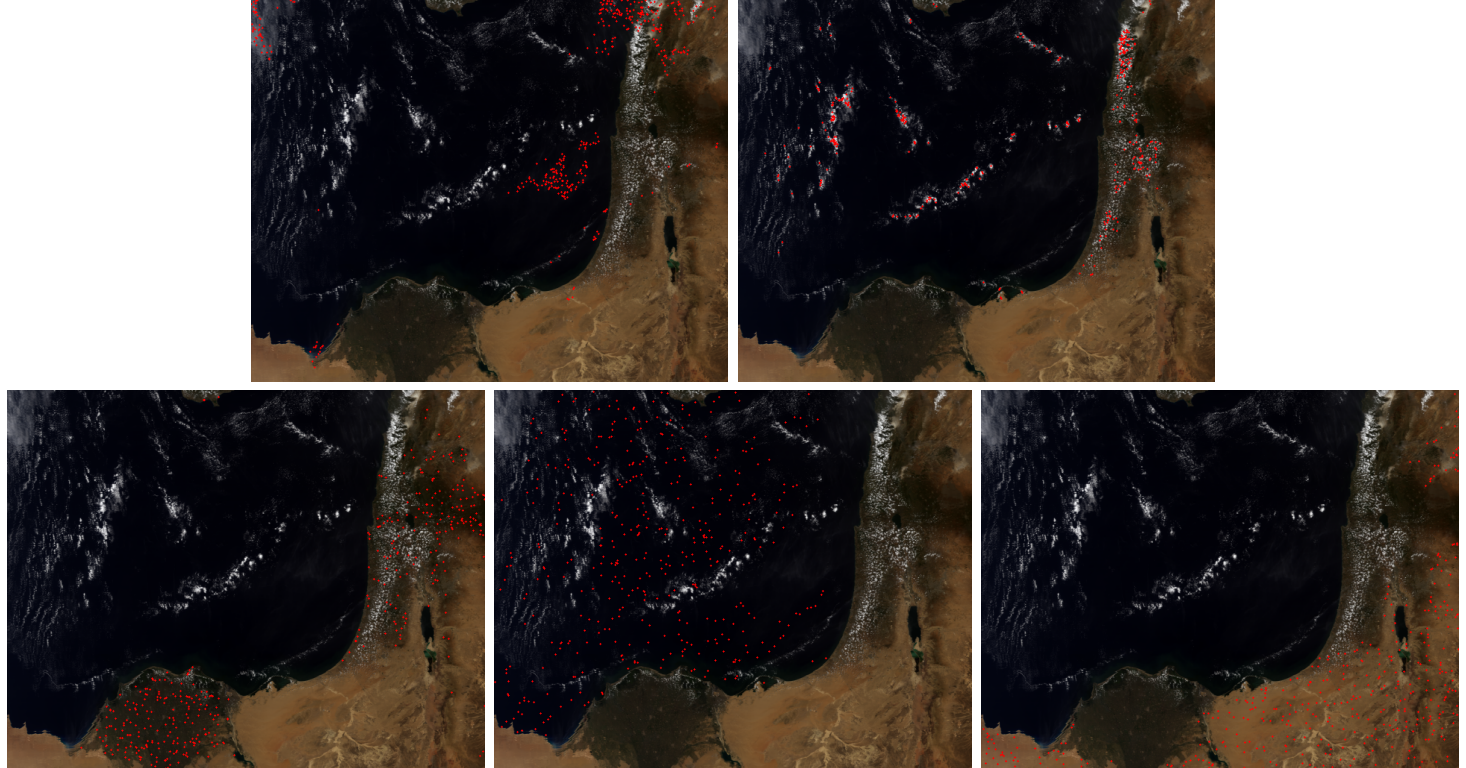


Figure 13: Pixels chosen from subsets of each threshold class mask. Top: ice cloud and water cloud samples. Bottom: vegetation, water, and arid land samples. Note that ice cloud samples include some pixels along the coast of Israel that correspond to water clouds with a very thin cirrus layer, as portrayed by the cloud phase RGB (Figure 12).

## 7 Samples from thresholded classes

---

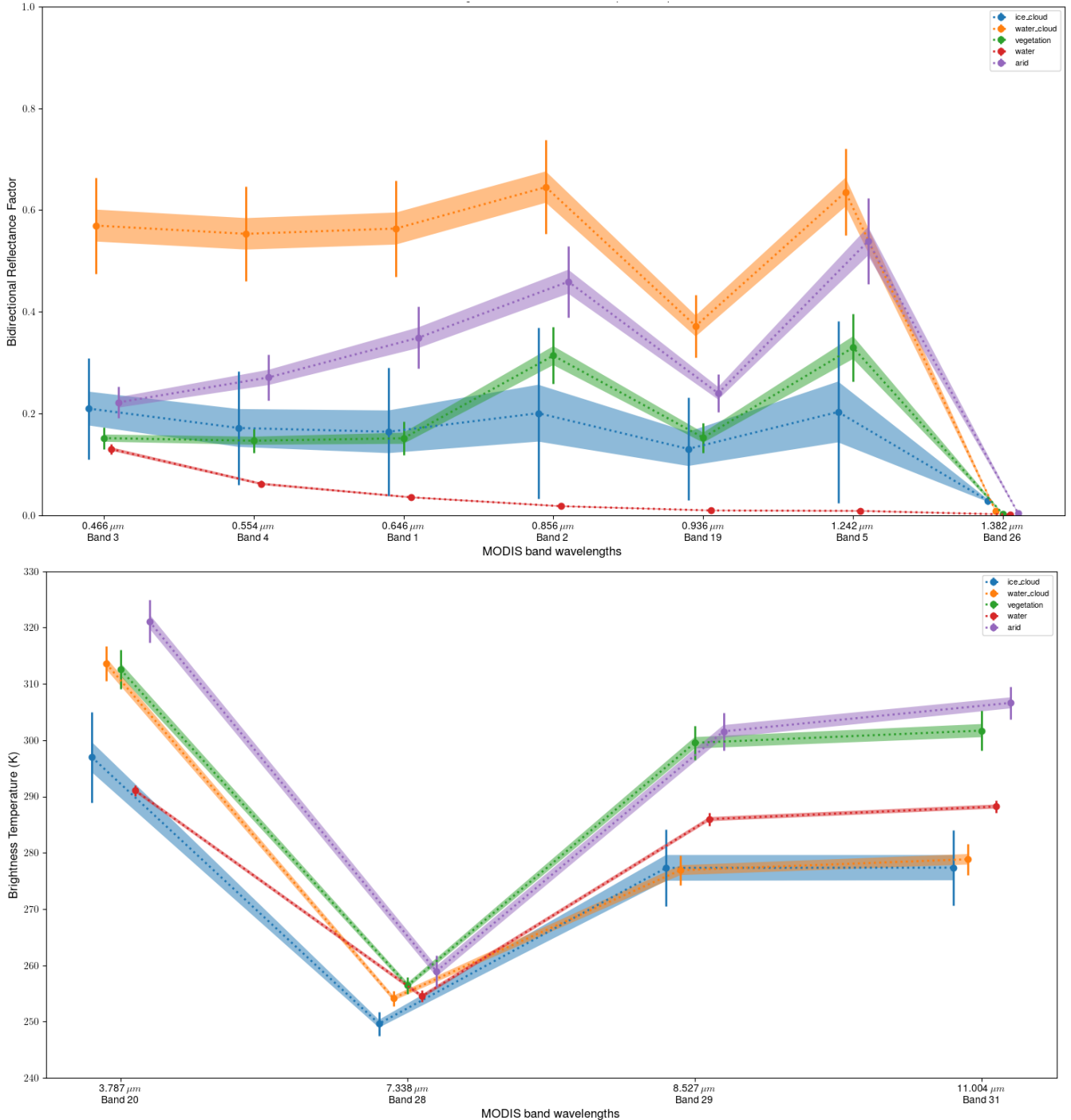


Figure 14: Top: spectral distribution of pixels in each class, sampled from threshold-derived class masks. The ice cloud class has by far the highest standard in each band due to the thresholding challenges mentioned previously. Nonetheless, this subset of thresholded pixels closely reflects the spectral distribution of the surface types in Figure 9.

7 Samples from thresholded classes

---

| $\lambda$   | $\mu$ | $\sigma$ | Reflectance Covariance ( $\times 10^4$ ) |       |       |       |       |       |      |
|-------------|-------|----------|--|-------|-------|-------|-------|-------|------|
| Ice Cloud   |       |          |  |       |       |       |       |       |      |
| 0.466       | 0.210 | 0.100    | 99.5                                     | 106.9 | 113.7 | 126.1 | 79.8  | 122.4 | 0.0  |
| 0.554       | 0.172 | 0.112    | 106.9                                    | 124.6 | 138.7 | 168.7 | 103.6 | 168.5 | 0.3  |
| 0.646       | 0.164 | 0.126    | 113.7                                    | 138.7 | 158.5 | 199.1 | 120.8 | 202.2 | 0.4  |
| 0.856       | 0.201 | 0.167    | 126.1                                    | 168.7 | 199.1 | 281.1 | 167.1 | 295.0 | 1.4  |
| 0.936       | 0.131 | 0.101    | 79.8                                     | 103.6 | 120.8 | 167.1 | 101.4 | 174.4 | 1.1  |
| 1.242       | 0.203 | 0.179    | 122.4                                    | 168.5 | 202.2 | 295.0 | 174.4 | 321.5 | 1.5  |
| 1.382       | 0.029 | 0.008    | 0.0                                      | 0.3   | 0.4   | 1.4   | 1.1   | 1.5   | 0.6  |
| Water Cloud |       |          |  |       |       |       |       |       |      |
| 0.466       | 0.564 | 0.094    | 89.2                                     | 82.8  | 87.2  | 87.3  | 66.0  | 47.4  | -0.4 |
| 0.554       | 0.645 | 0.092    | 82.8                                     | 85.4  | 78.3  | 80.7  | 72.0  | 52.2  | 0.5  |
| 0.646       | 0.570 | 0.094    | 87.2                                     | 78.3  | 89.1  | 86.8  | 61.0  | 42.3  | -1.0 |
| 0.856       | 0.553 | 0.093    | 87.3                                     | 80.7  | 86.8  | 86.2  | 63.9  | 45.7  | -0.5 |
| 0.936       | 0.635 | 0.085    | 66.0                                     | 72.0  | 61.0  | 63.9  | 72.6  | 46.0  | 0.9  |
| 1.242       | 0.372 | 0.062    | 47.4                                     | 52.2  | 42.3  | 45.7  | 46.0  | 38.3  | 1.4  |
| 1.382       | 0.009 | 0.006    | -0.4                                     | 0.5   | -1.0  | -0.5  | 0.9   | 1.4   | 0.3  |
| Vegetation  |       |          |  |       |       |       |       |       |      |
| 0.466       | 0.152 | 0.033    | 10.8                                     | 8.4   | 4.8   | 7.0   | 15.1  | 5.4   | 0.3  |
| 0.554       | 0.314 | 0.056    | 8.4                                      | 31.2  | 4.9   | 7.7   | 33.6  | 13.5  | 0.0  |
| 0.646       | 0.152 | 0.021    | 4.8                                      | 4.9   | 4.6   | 4.6   | 7.4   | 0.9   | -0.0 |
| 0.856       | 0.147 | 0.024    | 7.0                                      | 7.7   | 4.6   | 5.7   | 11.5  | 3.3   | 0.1  |
| 0.936       | 0.330 | 0.067    | 15.1                                     | 33.6  | 7.4   | 11.5  | 44.7  | 16.2  | 0.3  |
| 1.242       | 0.153 | 0.030    | 5.4                                      | 13.5  | 0.9   | 3.3   | 16.2  | 8.7   | 0.3  |
| 1.382       | 0.003 | 0.003    | 0.3                                      | 0.0   | -0.0  | 0.1   | 0.3   | 0.3   | 0.1  |
| Water       |       |          |  |       |       |       |       |       |      |
| 0.466       | 0.036 | 0.004    | 0.2                                      | 0.1   | 0.3   | 0.3   | 0.1   | 0.1   | 0.0  |
| 0.554       | 0.018 | 0.004    | 0.1                                      | 0.1   | 0.2   | 0.1   | 0.1   | 0.1   | 0.0  |
| 0.646       | 0.131 | 0.010    | 0.3                                      | 0.2   | 1.1   | 0.5   | 0.1   | 0.0   | -0.0 |
| 0.856       | 0.062 | 0.007    | 0.3                                      | 0.1   | 0.5   | 0.5   | 0.1   | 0.1   | 0.0  |
| 0.936       | 0.009 | 0.004    | 0.1                                      | 0.1   | 0.1   | 0.1   | 0.1   | 0.1   | 0.0  |
| 1.242       | 0.010 | 0.002    | 0.1                                      | 0.1   | 0.0   | 0.1   | 0.1   | 0.0   | 0.0  |
| 1.382       | 0.002 | 0.002    | 0.0                                      | 0.0   | -0.0  | 0.0   | 0.0   | 0.0   | 0.0  |
| Arid        |       |          |  |       |       |       |       |       |      |
| 0.466       | 0.349 | 0.061    | 37.3                                     | 41.6  | 16.5  | 26.5  | 47.5  | 14.6  | -0.4 |
| 0.554       | 0.459 | 0.071    | 41.6                                     | 49.9  | 18.5  | 29.6  | 56.9  | 16.4  | -0.6 |
| 0.646       | 0.222 | 0.031    | 16.5                                     | 18.5  | 9.4   | 13.1  | 20.8  | 4.6   | -0.3 |
| 0.856       | 0.271 | 0.045    | 26.5                                     | 29.6  | 13.1  | 20.1  | 33.4  | 9.7   | -0.3 |
| 0.936       | 0.539 | 0.085    | 47.5                                     | 56.9  | 20.8  | 33.4  | 71.6  | 20.1  | -0.6 |
| 1.242       | 0.240 | 0.037    | 14.6                                     | 16.4  | 4.6   | 9.7   | 20.1  | 13.7  | 0.4  |
| 1.382       | 0.005 | 0.003    | -0.4                                     | -0.6  | -0.3  | -0.3  | -0.6  | 0.4   | 0.1  |

Table 11: Mean values and standard deviations of reflectance pixels sampled from thresholded classes. Includes mean reflectance and standard deviation for each band and covariance matrices for the 5 surface types I identified.

## 7 Samples from thresholded classes

---

| $\lambda$   | $\mu$ | $\sigma$ | Brightness Temp. Covariance ( $\times 10^2$ ) |       |        |        |
|-------------|-------|----------|---|-------|--------|--------|
| Ice Cloud   |       |          |   |       |        |        |
| 3.79        | 297.0 | 8.04     | 6484.6  | 688.3 | 18.0   | 410.4  |
| 7.34        | 249.6 | 2.09     | 688.3   | 438.8 | 181.6  | 358.7  |
| 8.53        | 277.3 | 6.86     | 18.0  | 181.6 | 4712.9 | 4547.5 |
| 11.00       | 277.4 | 6.72     | 410.4   | 358.7 | 4547.5 | 4533.0 |
| Water Cloud |       |          |   |       |        |        |
| 3.79        | 313.6 | 3.07     | 942.3   | 216.7 | 341.8  | 380.8  |
| 7.34        | 254.2 | 1.35     | 216.7   | 183.3 | 242.5  | 280.3  |
| 8.53        | 276.9 | 2.62     | 341.8   | 242.5 | 687.8  | 714.4  |
| 11.00       | 278.8 | 2.79     | 380.8   | 280.3 | 714.4  | 781.0  |
| Vegetation  |       |          |   |       |        |        |
| 3.79        | 312.6 | 3.47     | 1210.5  | 273.0 | 844.8  | 1020.5 |
| 7.34        | 256.4 | 1.44     | 273.0   | 209.3 | 253.8  | 336.3  |
| 8.53        | 299.5 | 3.04     | 844.8   | 253.8 | 925.8  | 1022.5 |
| 11.00       | 301.7 | 3.50     | 1020.5  | 336.3 | 1022.5 | 1226.4 |
| Water       |       |          |   |       |        |        |
| 3.79        | 291.1 | 0.97     | 94.3  | 60.7  | 87.6   | 77.9   |
| 7.34        | 254.5 | 1.05     | 60.7  | 110.1 | 84.9   | 77.8   |
| 8.53        | 286.0 | 1.12     | 87.6  | 84.9  | 126.2  | 118.8  |
| 11.00       | 288.2 | 1.11     | 77.9  | 77.8  | 118.8  | 123.0  |
| Arid        |       |          |   |       |        |        |
| 3.79        | 321.1 | 3.80     | 1450.6  | 389.8 | -108.0 | 836.4  |
| 7.34        | 258.9 | 2.81     | 389.8   | 792.3 | 366.1  | 493.1  |
| 8.53        | 301.6 | 3.35     | -108.0  | 366.1 | 1123.1 | 424.3  |
| 11.00       | 306.6 | 2.93     | 836.4   | 493.1 | 424.3  | 859.3  |

Table 12: Mean values and standard deviations of brightness temperature pixels sampled from thresholded classes. Includes mean brightness temperature in Kelvin and standard deviation for each band and covariance matrices for the 5 surface types I identified.

|                         | Ice Cloud | Water Cloud | Vegetation | Water | Arid |
|-------------------------|-----------|-------------|------------|-------|------|
| Pixel Count             | 393       | 369         | 397        | 399   | 399  |
| Area (km <sup>2</sup> ) | 560       | 519         | 532        | 742   | 518  |

Table 13: Area and quantity of samples chosen from thresholded pixel classes. 400 random pixels were selected for each class, and repeated indeces were dropped. Although the same number of samples were selected for water and arid surfaces, the surface area of the water samples is much higher due to additional panoramic distortion on the left side of the image.

## 8 Maximum-likelihood classification with threshold samples

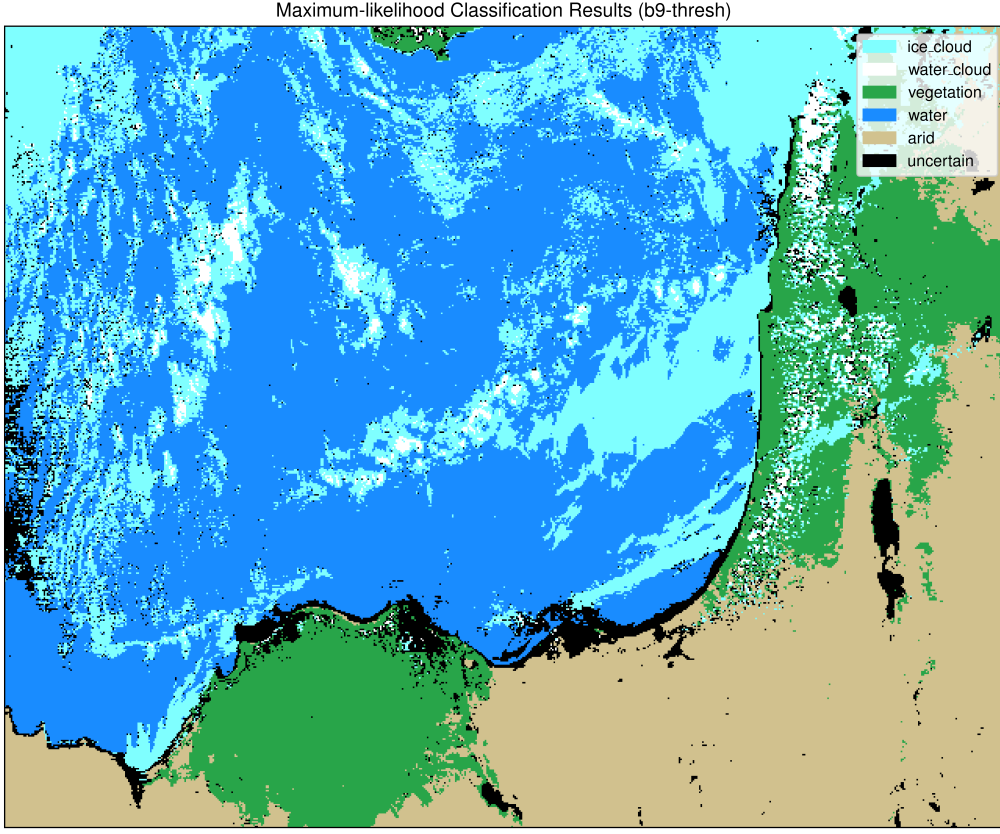


Figure 15: Results from maximum-likelihood classification using the threshold samples selected in Section 7. Pixels with a confidence less than 5% are added to the “uncertain” class. The left side also shows the effects of band 26 striping.

|                         | Ice Cloud | Water Cloud | Vegetation | Water  | Arid  | Uncertain |
|-------------------------|-----------|-------------|------------|--------|-------|-----------|
| Pixel Count             | 69620     | 5799        | 43344      | 125432 | 68670 | 14815     |
| Area (km <sup>2</sup> ) | 124604    | 8654        | 55828      | 226847 | 85326 | 27429     |

Table 14: Area and quantity of pixel classes identified with MLC using samples chosen from thresholded classes.

|                 | Ice Cloud | Water Cloud | Vegetation | Water | Arid  | Uncertain | Cons. Acc. |
|-----------------|-----------|-------------|------------|-------|-------|-----------|------------|
| MLC Ice Cloud   | 372       | 4           | 0          | 0     | 0     | 17        | 0.947      |
| MLC Water Cloud | 2         | 361         | 0          | 0     | 0     | 6         | 0.978      |
| MLC Vegetation  | 1         | 0           | 387        | 0     | 5     | 4         | 0.975      |
| MLC Water       | 0         | 0           | 0          | 395   | 0     | 4         | 0.990      |
| MLC Arid        | 0         | 0           | 9          | 0     | 385   | 5         | 0.965      |
| Prod. Acc.      | 0.992     | 0.989       | 0.977      | 1.000 | 0.987 |           |            |

Table 15: Confusion matrix comparing samples from manual thresholding to subsequent MLC results.

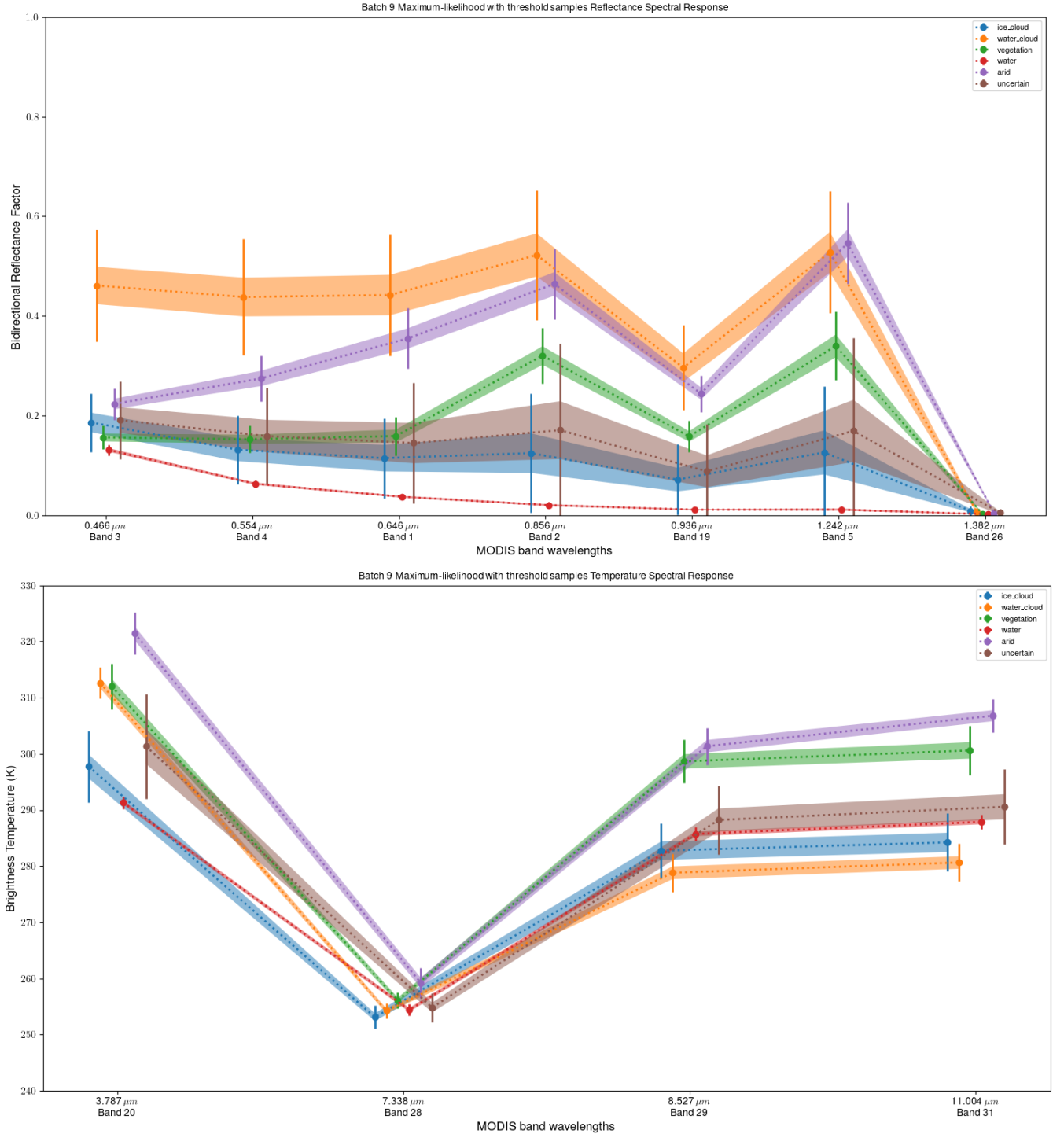


Figure 16: Spectral distribution of MLC classes for each input band, with class means derived from thresholded pixel samples. The uncertain class correlates extremely closely with the ice cloud class because the “uncertain” class is dominant in regions with low PWV, which enable enough reflectance transmission to imitate high cirrus clouds in vapor absorption bands like  $1.382\mu\text{m}$ .

| $\lambda$   | $\mu$ | $\sigma$ | Reflectance Covariance ( $\times 10^4$ ) |       |       |       |       |       |      |
|-------------|-------|----------|--|-------|-------|-------|-------|-------|------|
| Ice Cloud   |       |          |  |       |       |       |       |       |      |
| 0.466       | 0.187 | 0.059    | 34.3                                     | 37.7  | 40.7  | 50.9  | 29.4  | 54.3  | 0.3  |
| 0.554       | 0.132 | 0.069    | 37.7                                     | 47.3  | 54.2  | 75.0  | 43.8  | 81.4  | 1.2  |
| 0.646       | 0.115 | 0.080    | 40.7                                     | 54.2  | 63.9  | 91.2  | 53.5  | 100.0 | 1.8  |
| 0.856       | 0.125 | 0.119    | 50.9                                     | 75.0  | 91.2  | 141.8 | 82.9  | 156.7 | 3.3  |
| 0.936       | 0.072 | 0.070    | 29.4                                     | 43.8  | 53.5  | 82.9  | 49.7  | 91.5  | 2.7  |
| 1.242       | 0.126 | 0.132    | 54.3                                     | 81.4  | 100.0 | 156.7 | 91.5  | 175.2 | 3.5  |
| 1.382       | 0.009 | 0.010    | 0.3                                      | 1.2   | 1.8   | 3.3   | 2.7   | 3.5   | 1.0  |
| Water Cloud |       |          |  |       |       |       |       |       |      |
| 0.466       | 0.442 | 0.121    | 147.5                                    | 149.5 | 134.3 | 141.1 | 131.9 | 91.8  | 1.8  |
| 0.554       | 0.522 | 0.130    | 149.5                                    | 168.8 | 129.2 | 141.6 | 154.0 | 107.3 | 3.3  |
| 0.646       | 0.461 | 0.112    | 134.3                                    | 129.2 | 126.4 | 129.6 | 110.9 | 77.1  | 0.8  |
| 0.856       | 0.438 | 0.116    | 141.1                                    | 141.6 | 129.6 | 135.4 | 123.9 | 86.4  | 1.5  |
| 0.936       | 0.528 | 0.122    | 131.9                                    | 154.0 | 110.9 | 123.9 | 148.6 | 99.8  | 3.6  |
| 1.242       | 0.297 | 0.085    | 91.8                                     | 107.3 | 77.1  | 86.4  | 99.8  | 72.4  | 3.0  |
| 1.382       | 0.008 | 0.006    | 1.8                                      | 3.3   | 0.8   | 1.5   | 3.6   | 3.0   | 0.4  |
| Vegetation  |       |          |  |       |       |       |       |       |      |
| 0.466       | 0.159 | 0.039    | 15.0                                     | 11.3  | 6.7   | 9.9   | 18.8  | 6.9   | 0.5  |
| 0.554       | 0.321 | 0.056    | 11.3                                     | 31.2  | 5.8   | 9.2   | 35.3  | 14.6  | 0.2  |
| 0.646       | 0.156 | 0.024    | 6.7                                      | 5.8   | 5.6   | 5.9   | 8.6   | 1.6   | 0.1  |
| 0.856       | 0.153 | 0.027    | 9.9                                      | 9.2   | 5.9   | 7.6   | 13.6  | 4.4   | 0.2  |
| 0.936       | 0.340 | 0.069    | 18.8                                     | 35.3  | 8.6   | 13.6  | 46.9  | 18.2  | 0.6  |
| 1.242       | 0.158 | 0.032    | 6.9                                      | 14.6  | 1.6   | 4.4   | 18.2  | 10.0  | 0.5  |
| 1.382       | 0.003 | 0.004    | 0.5                                      | 0.2   | 0.1   | 0.2   | 0.6   | 0.5   | 0.1  |
| Water       |       |          |  |       |       |       |       |       |      |
| 0.466       | 0.038 | 0.006    | 0.3                                      | 0.3   | 0.4   | 0.4   | 0.3   | 0.2   | 0.0  |
| 0.554       | 0.021 | 0.006    | 0.3                                      | 0.3   | 0.3   | 0.3   | 0.4   | 0.2   | 0.1  |
| 0.646       | 0.131 | 0.011    | 0.4                                      | 0.3   | 1.2   | 0.6   | 0.2   | 0.1   | -0.0 |
| 0.856       | 0.064 | 0.007    | 0.4                                      | 0.3   | 0.6   | 0.5   | 0.3   | 0.1   | 0.0  |
| 0.936       | 0.012 | 0.006    | 0.3                                      | 0.4   | 0.2   | 0.3   | 0.4   | 0.2   | 0.1  |
| 1.242       | 0.012 | 0.004    | 0.2                                      | 0.2   | 0.1   | 0.1   | 0.2   | 0.1   | 0.1  |
| 1.382       | 0.003 | 0.003    | 0.0                                      | 0.1   | -0.0  | 0.0   | 0.1   | 0.1   | 0.1  |
| Arid        |       |          |  |       |       |       |       |       |      |
| 0.466       | 0.355 | 0.061    | 37.1                                     | 41.9  | 17.0  | 27.2  | 45.9  | 15.0  | -0.4 |
| 0.554       | 0.464 | 0.071    | 41.9                                     | 49.8  | 19.2  | 30.6  | 54.8  | 16.8  | -0.5 |
| 0.646       | 0.224 | 0.031    | 17.0                                     | 19.2  | 9.8   | 13.9  | 20.8  | 5.4   | -0.3 |
| 0.856       | 0.275 | 0.046    | 27.2                                     | 30.6  | 13.9  | 21.2  | 33.3  | 10.5  | -0.4 |
| 0.936       | 0.546 | 0.082    | 45.9                                     | 54.8  | 20.8  | 33.3  | 66.9  | 19.8  | -0.5 |
| 1.242       | 0.245 | 0.036    | 15.0                                     | 16.8  | 5.4   | 10.5  | 19.8  | 13.3  | 0.3  |
| 1.382       | 0.005 | 0.003    | -0.4                                     | -0.5  | -0.3  | -0.4  | -0.5  | 0.3   | 0.1  |

Table 16: Mean reflectance values and standard deviations of each reflectance band, for each class identified by MLC using pixel samples selected from band thresholds.

| $\lambda$   | $\mu$ | $\sigma$ | Brightness Temp. Covariance ( $\times 10^2$ ) |       |        |        |
|-------------|-------|----------|---|-------|--------|--------|
| Ice Cloud   |       |          |   |       |        |        |
| 3.79        | 297.7 | 6.38     | 4068.9  | 332.0 | 262.8  | 305.2  |
| 7.34        | 253.1 | 2.04     | 332.0   | 416.3 | 501.6  | 645.5  |
| 8.53        | 282.8 | 4.88     | 262.8   | 501.6 | 2384.7 | 2467.6 |
| 11.00       | 284.2 | 5.15     | 305.2   | 645.5 | 2467.6 | 2652.6 |
| Water Cloud |       |          |   |       |        |        |
| 3.79        | 312.6 | 2.79     | 775.9   | 150.9 | 200.9  | 179.8  |
| 7.34        | 254.2 | 1.29     | 150.9   | 166.1 | 271.4  | 292.2  |
| 8.53        | 278.8 | 3.38     | 200.9   | 271.4 | 1143.4 | 1106.7 |
| 11.00       | 280.6 | 3.35     | 179.8   | 292.2 | 1106.7 | 1119.1 |
| Vegetation  |       |          |   |       |        |        |
| 3.79        | 312.0 | 4.04     | 1634.5  | 320.6 | 1293.6 | 1486.3 |
| 7.34        | 256.1 | 1.38     | 320.6   | 189.6 | 344.3  | 408.9  |
| 8.53        | 298.7 | 3.88     | 1293.6  | 344.3 | 1502.7 | 1671.5 |
| 11.00       | 300.6 | 4.39     | 1486.3  | 408.9 | 1671.5 | 1926.1 |
| Water       |       |          |   |       |        |        |
| 3.79        | 291.3 | 1.09     | 117.8   | 47.3  | 74.1   | 57.0   |
| 7.34        | 254.4 | 1.07     | 47.3  | 114.9 | 90.8   | 87.3   |
| 8.53        | 285.8 | 1.20     | 74.1  | 90.8  | 144.7  | 145.0  |
| 11.00       | 287.9 | 1.28     | 57.0  | 87.3  | 145.0  | 163.5  |
| Arid        |       |          |   |       |        |        |
| 3.79        | 321.5 | 3.72     | 1386.7  | 355.0 | -158.1 | 827.1  |
| 7.34        | 259.2 | 2.72     | 355.0   | 739.6 | 343.6  | 478.9  |
| 8.53        | 301.4 | 3.28     | -158.1  | 343.6 | 1078.8 | 377.2  |
| 11.00       | 306.8 | 2.94     | 827.1   | 478.9 | 377.2  | 863.8  |

Table 17: Mean brightness temperature values and standard deviations of each emissive band, for each class identified by MLC using pixel samples from thresholds.

| $\lambda$ | $\mu$ | $\sigma$ | Reflectance Covariance ( $\times 10^4$ )      |        |        |        |       |       |
|-----------|-------|----------|---|--------|--------|--------|-------|-------|
| 0.466     | 0.145 | 0.121    | 147.0   | 200.1  | 83.0   | 115.5  | 204.5 | 109.3 |
| 0.554     | 0.171 | 0.174    | 200.1   | 302.4  | 107.4  | 154.8  | 316.6 | 163.6 |
| 0.646     | 0.191 | 0.078    | 83.0  | 107.4  | 60.1   | 70.5   | 104.4 | 59.7  |
| 0.856     | 0.159 | 0.097    | 115.5   | 154.8  | 70.5   | 94.3   | 155.0 | 85.0  |
| 0.936     | 0.170 | 0.187    | 204.5   | 316.6  | 104.4  | 155.0  | 348.6 | 169.9 |
| 1.242     | 0.088 | 0.095    | 109.3   | 163.6  | 59.7   | 85.0   | 169.9 | 91.0  |
| 1.382     | 0.005 | 0.008    | 4.1   | 5.7    | 2.1    | 3.2    | 5.8   | 3.6   |
| $\lambda$ | $\mu$ | $\sigma$ | Brightness Temp. Covariance ( $\times 10^2$ ) |        |        |        |       |       |
| 3.79      | 301.3 | 9.38     | 8802.7  | 881.8  | 3530.7 | 3898.1 |       |       |
| 7.34      | 254.8 | 2.59     | 881.8   | 673.2  | 1113.9 | 1227.8 |       |       |
| 8.53      | 288.2 | 6.16     | 3530.7  | 1113.9 | 3790.0 | 4043.4 |       |       |
| 11.00     | 290.6 | 6.69     | 3898.1  | 1227.8 | 4043.4 | 4480.2 |       |       |

Table 18: Reflectance and brightness temperature statistics for the uncertain class, which mostly included areas with high PWV and low clouds with cirrus cover, and regions over with no clouds and low PWV.

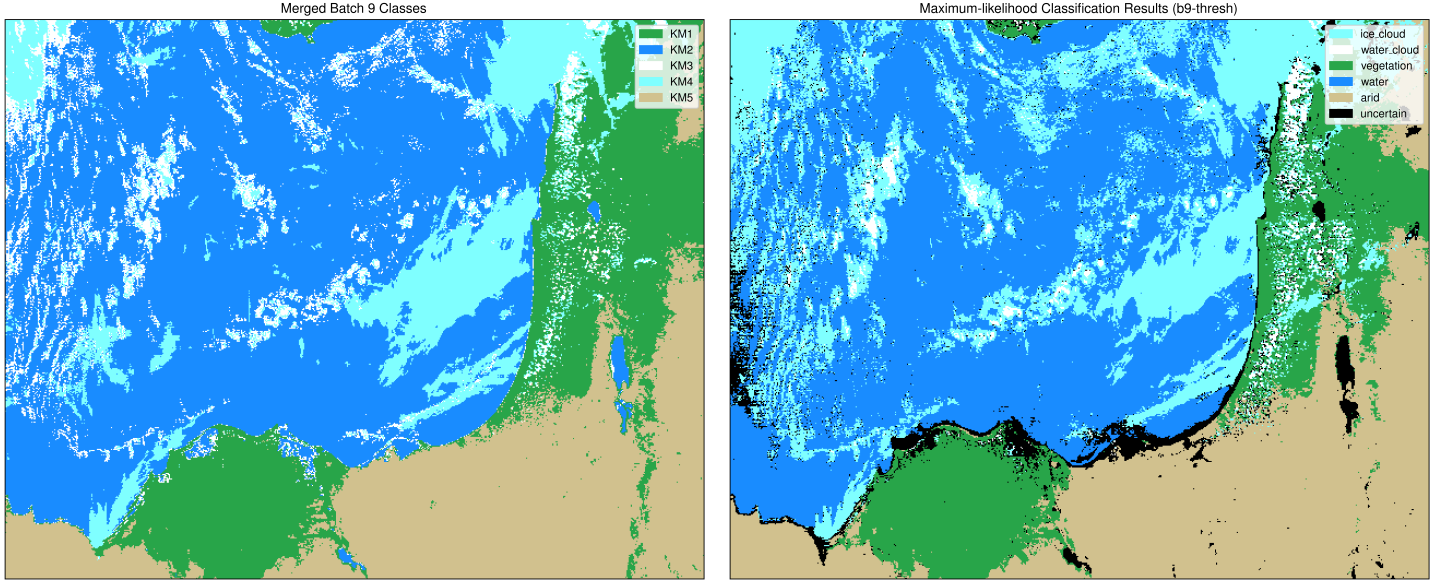


Figure 17: Left: K-means results. Right: maximum-likelihood results from threshold samples.

### Maximum-likelihood (thresholded samples) results analysis

Figure 15 and Table 14 show the results of supervised maximum-likelihood classification on my region, which was trained using the subset of  $\sim 400$  pixels selected for each class from the thresholded regions identified in Section 5. I executed MLC by passing pixel indeces and class labels to `subgrid.get_mlc` along with a list of bands for the channels I chose. This method returns an array of integers corresponding to each of the classes, with an optional “uncertain” class for pixels with discriminant function values outside of a provided confidence level.

Since I’m using 11 bands as inputs, my dataset has 11 degrees of freedom. The distance metric in the maximum-likelihood discriminant function conforms to a  $\chi^2$  distribution, so pixels with a discriminant value less than  $\chi = 17.275$  have a  $p$ -value, or confidence level, of less than .95. These pixels are assigned to the “uncertain” class, which helps characterize the behavior of the algorithm.

With subsets of my threshold regions as training samples, maximum-likelihood algorithm was conservative in classifying vegetation, and maintained low standard deviations for both the land and vegetation surface types. It was also confident in separating clouds from water, as the water class maintains very low variance for all input bands. Because of the challenges with cloud samples, MLC struggled to separate ice from water clouds.

Table 14 shows that the ice cloud class has the highest area and pixel count of all classes except for water, which is clear from the abundance of apparent ice clouds identified over the sea in Figure 15. Comparing the results to the daytime cloud phase RGB in Figure 12, an argument could be made that the high density of ice cloud surfaces identified on the left side of the maximum-likelihood results are valid, since the region is covered by a thin cirrus layer. Nonetheless, the ice clouds in this area are so thin that I suspect these clouds were misclassified mostly because of the high PWV above the water clouds. Also notice that the Dead Sea, and several water regions near the Nile Delta and in Israel were classified as “uncertain.” These areas are uniquely in regions with low PWV (Figure 5), which is evidence that atmospheric moisture is skewing classification

results.

Also notice the strong negative correlation of the  $8.53\mu\text{m}$  LWIR band with the  $3.79\mu\text{m}$  band in the arid surface class alone. The  $3.79\mu\text{m}$  band observes emissions as well as reflectance, and the  $8.53\mu\text{m}$  band correlates strongly with surface emissivity as covered in Section 4. The negative correlation between these bands is caused by the high reflectance and low emissivity of the arid and sandy regions surrounding the Nile Delta, Jordan, and the Southwest corner of Syria.

## 9 Samples from K-means classes

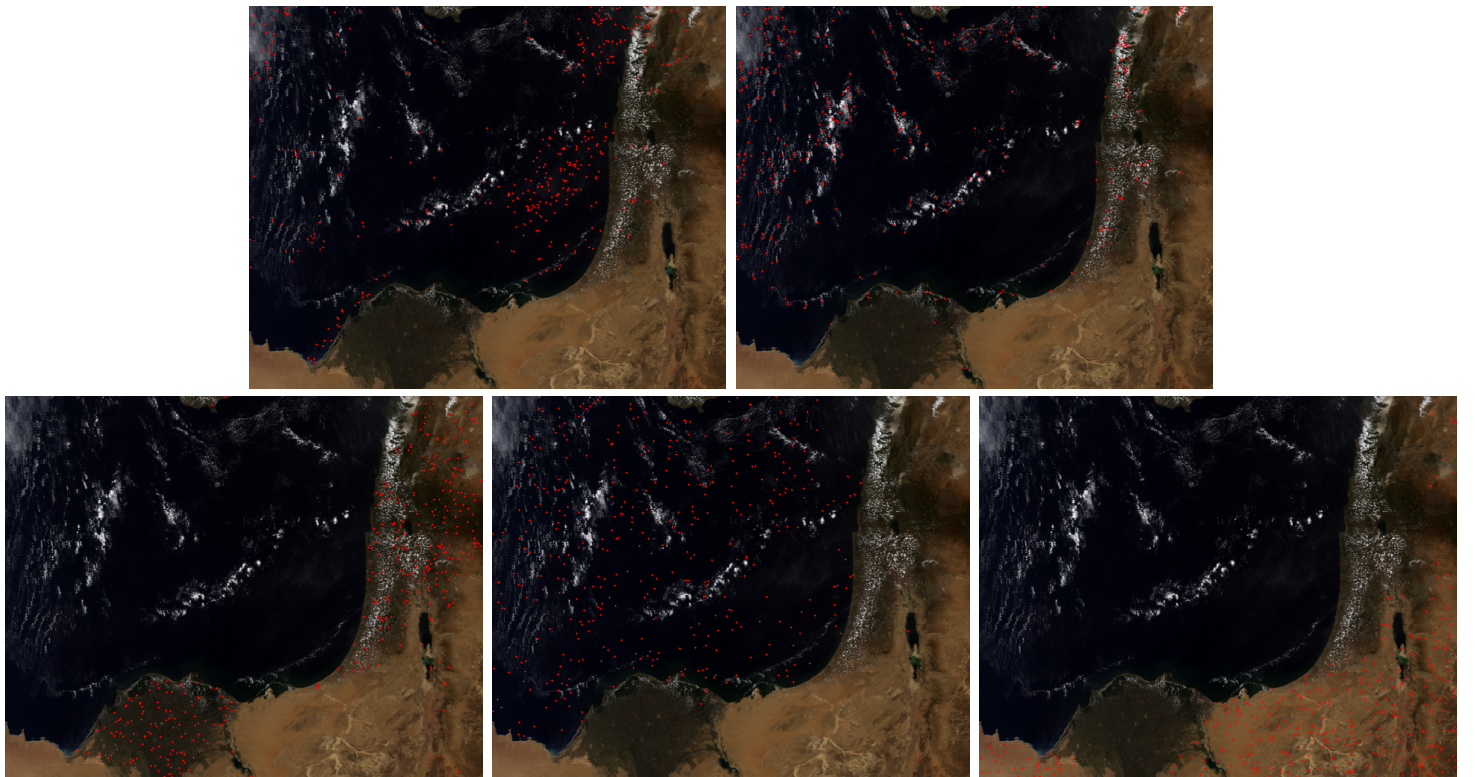


Figure 18: Pixels chosen from K-means masks for each class as samples for supervised maximum-likelihood classification. Top: KM4 (ice cloud), KM3 (water cloud). Bottom: KM1 (vegetation), KM2 (water), KM5 (arid)

|                         | KM1<br>(vegetation) | KM2<br>(water) | KM3<br>(water cloud) | KM4<br>(ice cloud) | KM5<br>(arid) |
|-------------------------|---------------------|----------------|----------------------|--------------------|---------------|
| Pixel Count             | 398                 | 400            | 396                  | 397                | 397           |
| Area (km <sup>2</sup> ) | 485                 | 747            | 846                  | 609                | 497           |

Table 19: Area and quantity of samples chosen from K-means pixel classes.

## 9 Samples from K-means classes

---

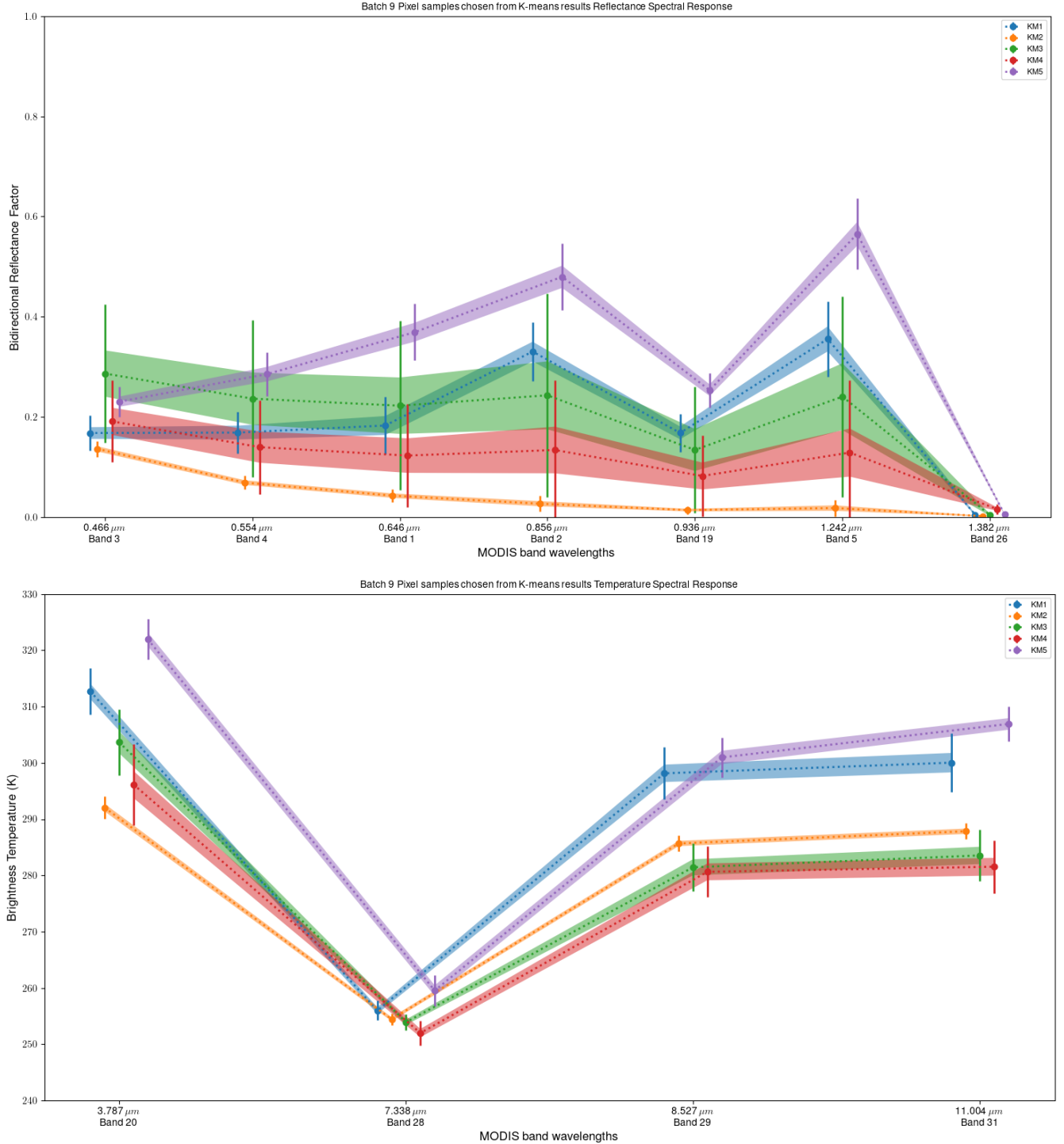


Figure 19: Spectral distribution of pixels sampled from K-means results to represent each class in maximum-likelihood classification. The spectral distribution curve and standard deviation curve of each sample class closely reflects the parent data (Figure 11). Unlike the restrictive thresholds, which had high standard deviations for ice clouds, water clouds have the highest standard deviation in the K-means subset. This is because many more thin and sub-pixel clouds with low reflectances were classified as water clouds rather than ice clouds by unsupervised K-means.

| $\lambda$         | $\mu$ | $\sigma$ | Reflectance Covariance ( $\times 10^4$ ) |       |       |       |       |       |      |  |
|-------------------|-------|----------|--|-------|-------|-------|-------|-------|------|--|
| KM1 (vegetation)  |       |          |  |       |       |       |       |       |      |  |
| 0.466             | 0.168 | 0.035    | 12.2                                     | 13.5  | 15.3  | 11.1  | 6.2   | 15.0  | 0.6  |  |
| 0.554             | 0.169 | 0.041    | 13.5                                     | 17.0  | 21.8  | 15.5  | 9.9   | 21.9  | 0.9  |  |
| 0.646             | 0.183 | 0.057    | 15.3                                     | 21.8  | 32.2  | 20.5  | 14.8  | 31.5  | 1.6  |  |
| 0.856             | 0.331 | 0.059    | 11.1                                     | 15.5  | 20.5  | 34.8  | 19.4  | 41.1  | 1.1  |  |
| 0.936             | 0.168 | 0.038    | 6.2                                      | 9.9   | 14.8  | 19.4  | 14.5  | 25.1  | 1.2  |  |
| 1.242             | 0.356 | 0.075    | 15.0                                     | 21.9  | 31.5  | 41.1  | 25.1  | 56.1  | 1.8  |  |
| 1.382             | 0.005 | 0.005    | 0.6                                      | 0.9   | 1.6   | 1.1   | 1.2   | 1.8   | 0.3  |  |
| KM2 (water)       |       |          |  |       |       |       |       |       |      |  |
| 0.466             | 0.043 | 0.013    | 1.8                                      | 2.1   | 1.7   | 1.8   | 2.1   | 1.0   | 0.0  |  |
| 0.554             | 0.027 | 0.016    | 2.1                                      | 2.4   | 1.7   | 2.0   | 2.5   | 1.2   | 0.0  |  |
| 0.646             | 0.136 | 0.016    | 1.7                                      | 1.7   | 2.4   | 1.8   | 1.7   | 0.8   | -0.0 |  |
| 0.856             | 0.069 | 0.014    | 1.8                                      | 2.0   | 1.8   | 1.9   | 2.0   | 0.9   | 0.0  |  |
| 0.936             | 0.018 | 0.016    | 2.1                                      | 2.5   | 1.7   | 2.0   | 2.7   | 1.2   | 0.1  |  |
| 1.242             | 0.014 | 0.008    | 1.0                                      | 1.2   | 0.8   | 0.9   | 1.2   | 0.6   | 0.1  |  |
| 1.382             | 0.002 | 0.002    | 0.0                                      | 0.0   | -0.0  | 0.0   | 0.1   | 0.1   | 0.1  |  |
| KM3 (water cloud) |       |          |  |       |       |       |       |       |      |  |
| 0.466             | 0.223 | 0.169    | 285.6                                    | 341.1 | 232.2 | 264.5 | 326.0 | 208.9 | 7.0  |  |
| 0.554             | 0.243 | 0.203    | 341.1                                    | 414.5 | 275.0 | 315.6 | 400.5 | 254.1 | 8.6  |  |
| 0.646             | 0.287 | 0.138    | 232.2                                    | 275.0 | 192.0 | 215.8 | 262.9 | 167.8 | 5.3  |  |
| 0.856             | 0.237 | 0.156    | 264.5                                    | 315.6 | 215.8 | 245.4 | 301.4 | 193.1 | 6.4  |  |
| 0.936             | 0.241 | 0.200    | 326.0                                    | 400.5 | 262.9 | 301.4 | 400.4 | 245.6 | 8.2  |  |
| 1.242             | 0.134 | 0.125    | 208.9                                    | 254.1 | 167.8 | 193.1 | 245.6 | 157.8 | 5.7  |  |
| 1.382             | 0.005 | 0.006    | 7.0                                      | 8.6   | 5.3   | 6.4   | 8.2   | 5.7   | 0.4  |  |
| KM4 (ice cloud)   |       |          |  |       |       |       |       |       |      |  |
| 0.466             | 0.123 | 0.103    | 107.0                                    | 139.1 | 80.3  | 96.2  | 137.9 | 78.5  | -0.4 |  |
| 0.554             | 0.134 | 0.140    | 139.1                                    | 195.4 | 98.3  | 123.4 | 197.9 | 111.2 | 0.6  |  |
| 0.646             | 0.191 | 0.082    | 80.3                                     | 98.3  | 66.7  | 74.4  | 97.7  | 54.4  | -1.2 |  |
| 0.856             | 0.140 | 0.093    | 96.2                                     | 123.4 | 74.4  | 87.4  | 122.3 | 69.2  | -0.6 |  |
| 0.936             | 0.129 | 0.144    | 137.9                                    | 197.9 | 97.7  | 122.3 | 207.7 | 112.5 | 0.8  |  |
| 1.242             | 0.082 | 0.080    | 78.5                                     | 111.2 | 54.4  | 69.2  | 112.5 | 64.7  | 1.1  |  |
| 1.382             | 0.016 | 0.010    | -0.4                                     | 0.6   | -1.2  | -0.6  | 0.8   | 1.1   | 1.0  |  |
| KM5 (arid)        |       |          |  |       |       |       |       |       |      |  |
| 0.466             | 0.369 | 0.057    | 32.1                                     | 36.7  | 14.8  | 23.6  | 36.3  | 11.7  | -0.3 |  |
| 0.554             | 0.480 | 0.067    | 36.7                                     | 44.4  | 16.9  | 26.9  | 44.4  | 13.0  | -0.5 |  |
| 0.646             | 0.231 | 0.030    | 14.8                                     | 16.9  | 9.2   | 12.5  | 16.3  | 4.1   | -0.2 |  |
| 0.856             | 0.286 | 0.043    | 23.6                                     | 26.9  | 12.5  | 18.8  | 26.2  | 8.1   | -0.3 |  |
| 0.936             | 0.565 | 0.071    | 36.3                                     | 44.4  | 16.3  | 26.2  | 50.4  | 13.4  | -0.6 |  |
| 1.242             | 0.253 | 0.035    | 11.7                                     | 13.0  | 4.1   | 8.1   | 13.4  | 12.0  | 0.4  |  |
| 1.382             | 0.005 | 0.004    | -0.3                                     | -0.5  | -0.2  | -0.3  | -0.6  | 0.4   | 0.1  |  |

Table 20: Reflectance band means, standard deviations, and covariance matrices for each of the surface types sampled from K-means results. Note the high variance values in the water cloud band due to abundance of water cloud pixels in K-means results.

| $\lambda$         | $\mu$ | $\sigma$ | Brightness | Temp. | Covariance ( $\times 10^2$ ) |         |
|-------------------|-------|----------|------------|-------|------------------------------|---------|
| KM1 (vegetation)  |       |          |            |       |                              |         |
| 3.79              | 312.7 | 4.10     | 1685.3     | 314.2 | 1303.2                       | 1523.8  |
| 7.34              | 256.0 | 1.73     | 314.2      | 300.9 | 410.4                        | 525.2   |
| 8.53              | 298.1 | 4.64     | 1303.2     | 410.4 | 2158.9                       | 2360.5  |
| 11.00             | 300.0 | 5.18     | 1523.8     | 525.2 | 2360.5                       | 2689.2  |
| KM2 (water)       |       |          |            |       |                              |         |
| 3.79              | 292.0 | 2.01     | 406.1      | 58.5  | 89.6                         | 76.4    |
| 7.34              | 254.5 | 1.06     | 58.5       | 112.2 | 96.9                         | 89.4    |
| 8.53              | 285.7 | 1.41     | 89.6       | 96.9  | 198.8                        | 194.2   |
| 11.00             | 287.8 | 1.43     | 76.4       | 89.4  | 194.2                        | 205.7   |
| KM3 (water cloud) |       |          |            |       |                              |         |
| 3.79              | 303.7 | 5.85     | 3428.4     | 103.2 | -941.2                       | -1023.6 |
| 7.34              | 253.9 | 1.42     | 103.2      | 202.4 | 354.6                        | 382.2   |
| 8.53              | 281.4 | 4.28     | -941.2     | 354.6 | 1836.7                       | 1961.1  |
| 11.00             | 283.6 | 4.60     | -1023.6    | 382.2 | 1961.1                       | 2123.0  |
| KM4 (ice cloud)   |       |          |            |       |                              |         |
| 3.79              | 296.2 | 7.20     | 5201.2     | 533.0 | -853.1                       | -646.2  |
| 7.34              | 252.0 | 2.21     | 533.0      | 489.8 | 455.0                        | 599.3   |
| 8.53              | 280.6 | 4.49     | -853.1     | 455.0 | 2019.8                       | 2082.2  |
| 11.00             | 281.5 | 4.72     | -646.2     | 599.3 | 2082.2                       | 2234.2  |
| KM5 (arid)        |       |          |            |       |                              |         |
| 3.79              | 322.0 | 3.63     | 1321.8     | 270.2 | -203.2                       | 767.7   |
| 7.34              | 259.5 | 2.79     | 270.2      | 782.2 | 489.4                        | 516.5   |
| 8.53              | 301.0 | 3.56     | -203.2     | 489.4 | 1270.3                       | 480.4   |
| 11.00             | 306.9 | 3.08     | 767.7      | 516.5 | 480.4                        | 953.2   |

Table 21: Emissive band mean brightness temperatures, standard deviations, and covariance matrices for each of the surface types sampled from K-means results. Notice that since ice cloud samples taken from the K-means results include fewer mid-level clouds over the coast of Israel, and more optically thick cirrus over water. This is why the  $3.79\mu m$  band, which senses reflectance, has a high variance within the class. The  $3.79\mu m$  band also has a negative covariance with respect to both water and ice clouds because more reflective clouds are generally colder.

## 10 Maximum-likelihood classification with K-means samples

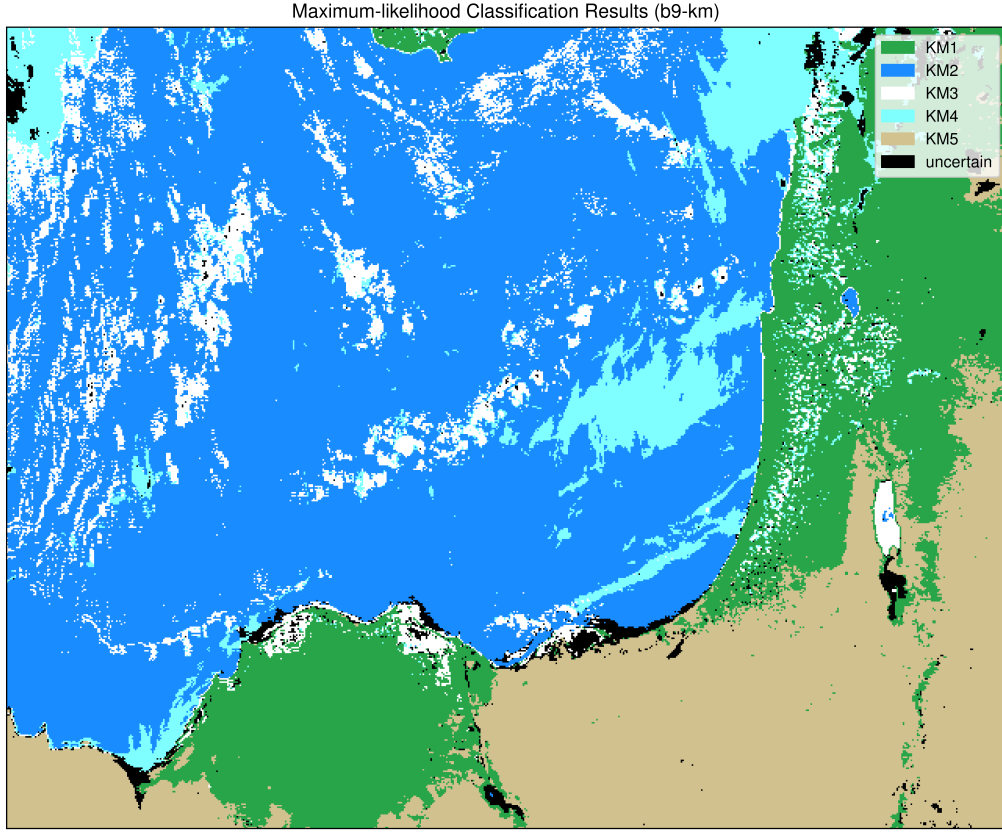


Figure 20: Results from maximum-likelihood classification using class samples selected from K-means classes. Pixels with a confidence level less than 5% are assigned to the “uncertain” class.

|                         | MLC1<br>(vegetation) | MLC2<br>(water) | MLC3<br>(water cloud) | MLC4<br>(ice cloud) | MLC5<br>(arid) | Uncertain |
|-------------------------|----------------------|-----------------|-----------------------|---------------------|----------------|-----------|
| Pixel Count             | 58,435               | 155,717         | 24,430                | 22,898              | 61,084         | 5,116     |
| Area (km <sup>2</sup> ) | 71,943               | 287,288         | 49,023                | 35,537              | 77,089         | 7,806     |

Table 22: Area and quantity of pixel classes from maximum-likelihood classification using K-means samples chosen from K-means classes. The amount of vegetation identified has increased compared to the threshold-trained maximum-likelihood results, and the number of ice cloud pixels identified decreased significantly from 69,620 to 22,898.

|            | KM1   | KM2   | KM3   | KM4   | KM5   | Uncertain | Cons. Acc. |
|------------|-------|-------|-------|-------|-------|-----------|------------|
| MLC1       | 375   | 0     | 2     | 6     | 9     | 6         | 0.942      |
| MLC2       | 0     | 384   | 13    | 1     | 0     | 2         | 0.960      |
| MLC3       | 6     | 16    | 337   | 23    | 0     | 14        | 0.851      |
| MLC4       | 6     | 104   | 48    | 219   | 0     | 20        | 0.552      |
| MLC5       | 11    | 0     | 0     | 0     | 383   | 3         | 0.965      |
| Prod. Acc. | 0.942 | 0.762 | 0.843 | 0.880 | 0.977 |           |            |

Table 23: Confusion matrix comparing K-means samples to subsequent MLC results.

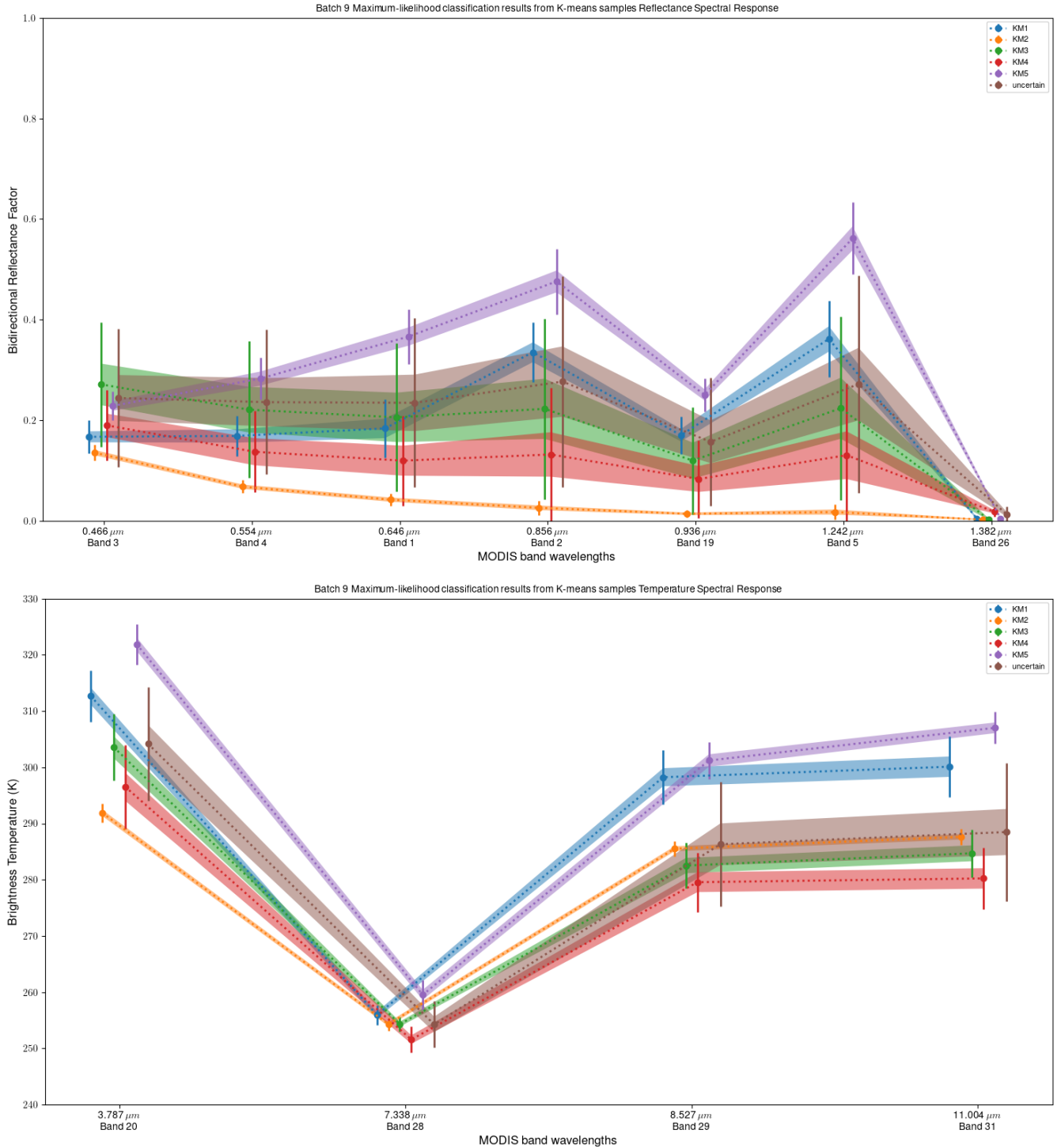


Figure 21: Spectral distribution of each class identified by MLC using K-means pixel samples. Like the sampled pixels that were used as inputs (Figure 19), the highest standard deviations are between the ice cloud (MLC4) and water cloud (MLC5) classes. Unsurprisingly, the “Uncertain” class dominantly correlates with the ice cloud and water cloud classes, however many of the uncertain regions are actually over water. I believe this is because the infrared spectral signature for water in clear-sky areas is similar to that of highly reflective water clouds.

| $\lambda$          | $\mu$ | $\sigma$ | Reflectance Covariance ( $\times 10^4$ ) |       |       |       |       |       |      |  |
|--------------------|-------|----------|--|-------|-------|-------|-------|-------|------|--|
| MLC1 (vegetation)  |       |          |  |       |       |       |       |       |      |  |
| 0.466              | 0.167 | 0.033    | 10.7                                     | 12.0  | 14.4  | 10.9  | 5.6   | 15.0  | 0.5  |  |
| 0.554              | 0.169 | 0.040    | 12.0                                     | 15.9  | 21.7  | 16.4  | 9.8   | 23.3  | 0.8  |  |
| 0.646              | 0.184 | 0.058    | 14.4                                     | 21.7  | 33.4  | 22.2  | 15.2  | 34.1  | 1.3  |  |
| 0.856              | 0.335 | 0.059    | 10.9                                     | 16.4  | 22.2  | 34.8  | 18.5  | 41.7  | 0.7  |  |
| 0.936              | 0.170 | 0.037    | 5.6                                      | 9.8   | 15.2  | 18.5  | 13.7  | 24.2  | 1.0  |  |
| 1.242              | 0.362 | 0.076    | 15.0                                     | 23.3  | 34.1  | 41.7  | 24.2  | 57.2  | 1.3  |  |
| 1.382              | 0.005 | 0.005    | 0.5                                      | 0.8   | 1.3   | 0.7   | 1.0   | 1.3   | 0.3  |  |
| MLC2 (water)       |       |          |  |       |       |       |       |       |      |  |
| 0.466              | 0.042 | 0.013    | 1.6                                      | 1.7   | 1.6   | 1.6   | 1.9   | 0.8   | 0.0  |  |
| 0.554              | 0.026 | 0.014    | 1.7                                      | 2.0   | 1.6   | 1.6   | 2.1   | 1.0   | 0.1  |  |
| 0.646              | 0.136 | 0.016    | 1.6                                      | 1.6   | 2.5   | 1.8   | 1.7   | 0.7   | -0.1 |  |
| 0.856              | 0.068 | 0.013    | 1.6                                      | 1.6   | 1.8   | 1.7   | 1.8   | 0.8   | 0.0  |  |
| 0.936              | 0.018 | 0.015    | 1.9                                      | 2.1   | 1.7   | 1.8   | 2.4   | 1.1   | 0.1  |  |
| 1.242              | 0.014 | 0.007    | 0.8                                      | 1.0   | 0.7   | 0.8   | 1.1   | 0.5   | 0.1  |  |
| 1.382              | 0.003 | 0.003    | 0.0                                      | 0.1   | -0.1  | 0.0   | 0.1   | 0.1   | 0.1  |  |
| MLC3 (water cloud) |       |          |  |       |       |       |       |       |      |  |
| 0.466              | 0.206 | 0.147    | 216.6                                    | 262.0 | 180.4 | 200.1 | 263.1 | 154.1 | 3.8  |  |
| 0.554              | 0.223 | 0.179    | 262.0                                    | 321.7 | 216.0 | 241.6 | 324.2 | 190.0 | 4.9  |  |
| 0.646              | 0.272 | 0.124    | 180.4                                    | 216.0 | 152.9 | 167.1 | 216.4 | 126.3 | 2.9  |  |
| 0.856              | 0.221 | 0.136    | 200.1                                    | 241.6 | 167.1 | 185.1 | 242.2 | 141.9 | 3.4  |  |
| 0.936              | 0.224 | 0.182    | 263.1                                    | 324.2 | 216.4 | 242.2 | 331.2 | 191.9 | 5.0  |  |
| 1.242              | 0.120 | 0.107    | 154.1                                    | 190.0 | 126.3 | 141.9 | 191.9 | 113.8 | 3.2  |  |
| 1.382              | 0.003 | 0.005    | 3.8                                      | 4.9   | 2.9   | 3.4   | 5.0   | 3.2   | 0.2  |  |
| MLC4 (ice cloud)   |       |          |  |       |       |       |       |       |      |  |
| 0.466              | 0.120 | 0.089    | 79.9                                     | 114.6 | 58.7  | 71.7  | 121.9 | 66.7  | -0.1 |  |
| 0.554              | 0.132 | 0.132    | 114.6                                    | 175.4 | 78.7  | 101.5 | 187.5 | 101.2 | 0.1  |  |
| 0.646              | 0.190 | 0.070    | 58.7                                     | 78.7  | 48.8  | 54.6  | 83.8  | 45.9  | -0.5 |  |
| 0.856              | 0.138 | 0.081    | 71.7                                     | 101.5 | 54.6  | 65.2  | 108.0 | 59.0  | -0.2 |  |
| 0.936              | 0.131 | 0.142    | 121.9                                    | 187.5 | 83.8  | 108.0 | 202.1 | 108.0 | -0.1 |  |
| 1.242              | 0.084 | 0.077    | 66.7                                     | 101.2 | 45.9  | 59.0  | 108.0 | 59.3  | 0.6  |  |
| 1.382              | 0.018 | 0.009    | -0.1                                     | 0.1   | -0.5  | -0.2  | -0.1  | 0.6   | 0.9  |  |
| MLC5 (arid)        |       |          |  |       |       |       |       |       |      |  |
| 0.466              | 0.367 | 0.054    | 29.6                                     | 34.7  | 13.9  | 22.0  | 35.2  | 10.4  | -0.4 |  |
| 0.554              | 0.476 | 0.065    | 34.7                                     | 42.3  | 16.3  | 25.6  | 43.6  | 11.9  | -0.6 |  |
| 0.646              | 0.229 | 0.029    | 13.9                                     | 16.3  | 8.5   | 11.7  | 16.4  | 3.7   | -0.3 |  |
| 0.856              | 0.283 | 0.042    | 22.0                                     | 25.6  | 11.7  | 17.6  | 25.8  | 7.4   | -0.4 |  |
| 0.936              | 0.562 | 0.071    | 35.2                                     | 43.6  | 16.4  | 25.8  | 51.1  | 13.0  | -0.5 |  |
| 1.242              | 0.251 | 0.033    | 10.4                                     | 11.9  | 3.7   | 7.4   | 13.0  | 11.0  | 0.4  |  |
| 1.382              | 0.005 | 0.003    | -0.4                                     | -0.6  | -0.3  | -0.4  | -0.5  | 0.4   | 0.1  |  |

Table 24: Reflectance means, standard deviations, and covariance matrices for each class identified by MLC using samples from K-means results. Once again, water and vegetation pixels were well masked and have generally low standard deviations. Band correlations for cloud surfaces have much higher variances and nearby means, which suggests uncertainty in their designation.

| $\lambda$          | $\mu$ | $\sigma$ | Brightness | Temp. | Covariance ( $\times 10^2$ ) |         |
|--------------------|-------|----------|------------|-------|------------------------------|---------|
| MLC1 (vegetation)  |       |          |            |       |                              |         |
| 3.79               | 312.7 | 4.55     | 2073.3     | 447.9 | 1684.4                       | 1947.3  |
| 7.34               | 255.9 | 1.76     | 447.9      | 308.2 | 541.8                        | 657.6   |
| 8.53               | 298.2 | 4.81     | 1684.4     | 541.8 | 2317.0                       | 2579.9  |
| 11.00              | 300.1 | 5.44     | 1947.3     | 657.6 | 2579.9                       | 2957.5  |
| MLC2 (water)       |       |          |            |       |                              |         |
| 3.79               | 291.9 | 1.68     | 281.2      | 26.2  | 16.1                         | 2.0     |
| 7.34               | 254.3 | 1.12     | 26.2       | 126.0 | 104.7                        | 102.4   |
| 8.53               | 285.5 | 1.33     | 16.1       | 104.7 | 176.4                        | 178.0   |
| 11.00              | 287.6 | 1.42     | 2.0        | 102.4 | 178.0                        | 201.0   |
| MLC3 (water cloud) |       |          |            |       |                              |         |
| 3.79               | 303.6 | 5.89     | 3464.0     | 22.8  | -1246.9                      | -1344.6 |
| 7.34               | 254.3 | 1.32     | 22.8       | 173.9 | 311.9                        | 317.7   |
| 8.53               | 282.5 | 4.08     | -1246.9    | 311.9 | 1663.4                       | 1712.0  |
| 11.00              | 284.7 | 4.23     | -1344.6    | 317.7 | 1712.0                       | 1787.1  |
| MLC4 (ice cloud)   |       |          |            |       |                              |         |
| 3.79               | 296.6 | 7.48     | 5598.9     | 742.4 | -849.9                       | -645.4  |
| 7.34               | 251.6 | 2.27     | 742.4      | 514.4 | 530.5                        | 680.7   |
| 8.53               | 279.6 | 5.29     | -849.9     | 530.5 | 2798.8                       | 2840.6  |
| 11.00              | 280.2 | 5.44     | -645.4     | 680.7 | 2840.6                       | 2964.9  |
| MLC5 (arid)        |       |          |            |       |                              |         |
| 3.79               | 321.9 | 3.61     | 1302.8     | 265.5 | -195.0                       | 753.4   |
| 7.34               | 259.5 | 2.65     | 265.5      | 704.8 | 417.3                        | 449.5   |
| 8.53               | 301.2 | 3.30     | -195.0     | 417.3 | 1091.7                       | 356.6   |
| 11.00              | 307.0 | 2.84     | 753.4      | 449.5 | 356.6                        | 809.4   |

Table 25: Brightness temperature means and standard deviations for each class identified by MLC with samples from K-means results.

| $\lambda$ | $\mu$ | $\sigma$ | Reflectance Covariance ( $\times 10^4$ )      |        |         |         |       |       |      |
|-----------|-------|----------|---|--------|---------|---------|-------|-------|------|
| 0.466     | 0.235 | 0.168    | 282.5   | 334.6  | 210.9   | 235.9   | 318.1 | 201.4 | 7.8  |
| 0.554     | 0.277 | 0.210    | 334.6   | 439.3  | 235.1   | 270.2   | 433.1 | 259.2 | 11.8 |
| 0.646     | 0.244 | 0.137    | 210.9   | 235.1  | 187.2   | 191.6   | 214.0 | 148.8 | 7.0  |
| 0.856     | 0.236 | 0.144    | 235.9   | 270.2  | 191.6   | 206.6   | 249.6 | 165.6 | 6.6  |
| 0.936     | 0.272 | 0.216    | 318.1   | 433.1  | 214.0   | 249.6   | 467.5 | 254.2 | 12.2 |
| 1.242     | 0.157 | 0.127    | 201.4   | 259.2  | 148.8   | 165.6   | 254.2 | 161.3 | 9.1  |
| 1.382     | 0.014 | 0.015    | 7.8   | 11.8   | 7.0     | 6.6     | 12.2  | 9.1   | 2.2  |
| $\lambda$ | $\mu$ | $\sigma$ | Brightness Temp. Covariance ( $\times 10^2$ ) |        |         |         |       |       |      |
| 3.79      | 304.2 | 10.11    | 10215.1                                       | 1242.3 | 4219.0  | 5408.5  |       |       |      |
| 7.34      | 254.3 | 4.13     | 1242.3  | 1706.9 | 3105.3  | 3723.4  |       |       |      |
| 8.53      | 286.3 | 11.10    | 4219.0  | 3105.3 | 12328.1 | 13482.3 |       |       |      |
| 11.00     | 288.5 | 12.30    | 5408.5  | 3723.4 | 13482.3 | 15132.9 |       |       |      |

Table 26: Reflectance and brightness temperature statistics of “uncertain” class pixels with discriminant function values  $\chi < 19.675$

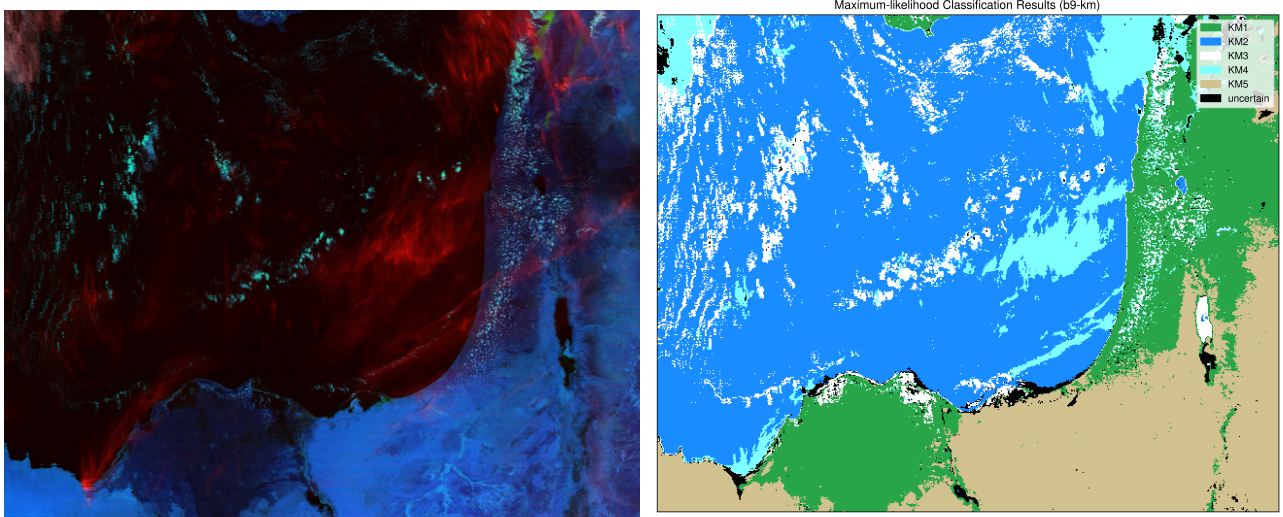


Figure 22: Comparison between day cloud-phase RGB and MLC results from K-means class samples.

### Maximum-likelihood (K-means samples) results analysis

Compared to the threshold-derived MLC results, MLC classification with K-means samples was more hesitant to classify low-reflectance pixels as ice clouds. The small sub-pixel water clouds on the left side of the region were classified as water clouds, which brought out a feature like cumulus streets. These results demonstrate a new challenge, which is that water surfaces in clear-sky regions are misclassified as uncertain or water clouds.

According to Table 23, water and ice cloud classes have the lowest consumer accuracies, which is corroborated by their high standard deviations and nearby means throughout the reflectance bands. Water, however, has the lowest consumer accuracy due to misclassified regions near the Nile Delta and the Dead Sea. The spectral response curves in Figure 21 shows that the uncertain class correlates best with the brightest ice and water clouds in the reflectance bands, but has an infrared response curve that more closely imitates the response curve of water.

Many of the water pixels misclassified as water clouds are in areas that have more sediment, and higher reflectance overall. These regions weren't well represented by the 400 pixel samples obtained from K-means, so I believe their relatively high reflectance and cool temperatures made their spectral signature similar to thin water clouds. The mean  $11\mu m$  LWIR window brightness temperature for the water class is  $287.8K$ , which is similar to the  $283.6K$  mean for water clouds.

## 11 Conclusion

Figure 23 shows all classification results obtained during this analysis. The main difficulties I encountered in classification were faulty data due to striping, an abundance of optically thin cloud pixels, and a steep gradient of precipitable water vapor across the region I studied. With the 7 reflectance bands and 4 thermal bands I chose, I found that ice and water clouds were difficult to separate under these conditions. After considerable experimentation with K-means, I determined that water and ice clouds were only consistently separated if the image was classified using 10 centroids, then manually merged to the appropriate surface types.

My custom thresholding technique attempted to assign tight thresholds on ice and water clouds, but the ice cloud sample was biased by several mid-level clouds covered by a thin cirrus layer in a dry environment. This resulted in apparent over-classification of ice clouds, and low confidence in classifying water pixels in dry environments. Unsupervised K-means classification was more conservative in classifying water clouds, and has the most agreeable results overall, in my opinion. Maximum-likelihood classification mimicked the K-means water and ice cloud surface distribution when provided with samples from the unsupervised results, but once again misclassified or had low confidence for water surfaces in dry environments.

I only used normalized brightness temperature and reflectance data values as inputs for the classification algorithms, but I suspect that using scalar composites like NDWI would have prevented some of the ambiguity between water and water clouds in the K-means results and the results from MLC with K-means samples. Furthermore, I didn't include the NIR  $1.64\mu m$  cloud phase band because it was seriously corrupted by striping, and because most of the ice clouds in my image were too optically thin to be meaningfully characterized by the band. In other scenes, inclusion of this band may have made ice clouds much easier to distinguish from water clouds.

Future work for this project includes the continued development of my Python package, including the implementation of an atmospheric correction procedure, which could have resolved many of the classification challenges encountered in this report. I also intend to adapt the MOD021KM class into a more abstract parent class that implements the same dynamic recipe evaluation system as the MOD021KM class.

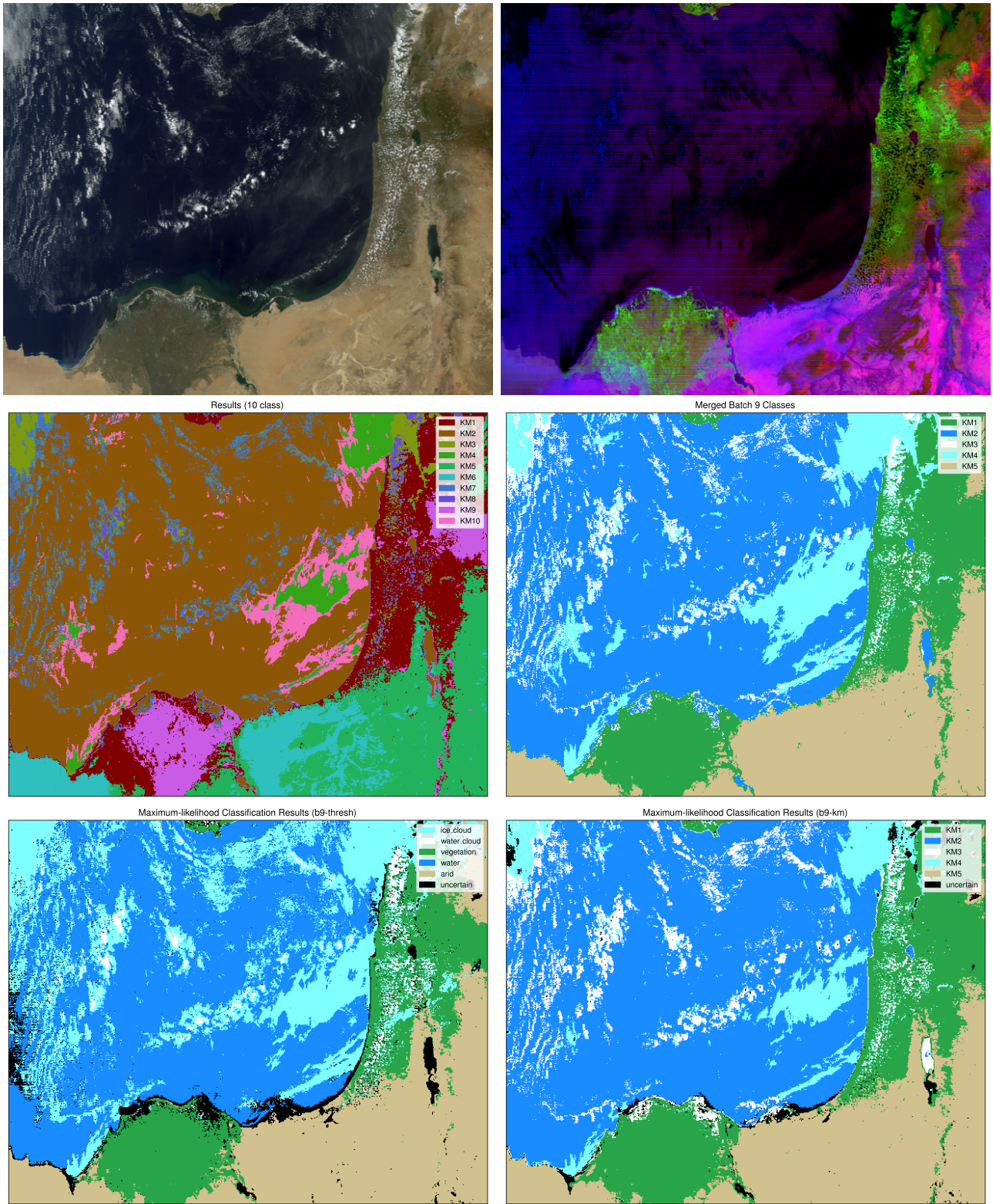


Figure 23: Top: truecolor and custom RGBs. Middle: 10-class and merged 5-class K-means results. Bottom: MLC results sampled from thresholds and K-means, respectively.

## References

- [1] Flasse and Ceccato, “A contextual algorithm for avhrr fire detection,” *International Journal of Remote Sensing*, vol. 17, 1996.
- [2] “Next generation satellite rgb dust imagery leads to operational changes at nws albuquerue,” *J. Operational Meteor.*, vol. 4.
- [3] J. Torres, S. Lindstrom, and A. Heidinger, “Goes-r abi day cloud type rgb quick guide,” November 2021.
- [4] J. Li, T. Schmit, X. Jin, and G. Martin, “Goes-r advanced baseline imager algorithm theoretical basis document for legacy atmospheric moisture profile,” July.
- [5] Platnick, Meyer, and King, “Cloud optical properties user’s guide for c6 & c6.1,” 7 2018.
- [6] A. V. D. Griend and M. Owe, “On the relationship between thermal emissivity and the normalized difference vegetation index for natural surfaces,” *International Journal of Remote Sensing*, vol. 14, October.
- [7] S. Mumford, ed., *Compact World Atlas*. Penguin Random House, 7 ed., 2001.
- [8] S. Mineo and G. Pappalardo, “Rock emissivity measurement for infrared thermography engineering geological applications,” *Applied Sciences*, April 2021.
- [9] B. Shimron, A. Eyal, and B. Y., “Sinai geological map. aeromagnetic map,”